

1 **Airborne bacteria viability and air quality: a protocol to quantitatively investigate the**
2 **possible correlation by an atmospheric simulation chamber**

3
4 *Virginia Vernocchi¹, Elena Abd El^{1,2}, Marco Brunoldi^{1,2}, Silvia Giulia Danelli¹, Elena Gatta²,*
5 *Tommaso Isolabella^{1,2}, Federico Mazzei^{1,2*}, Franco Parodi¹, Paolo Prati^{1,2}, Dario Massabò^{1,2}*

6
7 ¹ INFN, Sezione di Genova, via Dodecaneso 33, 16146 Genova, Italy

8 ² Dipartimento di Fisica, Università di Genova, via Dodecaneso 33, 16146 Genova, Italy

9
10 *Keywords:* measure technique for bioaerosol, airborne bacteria, Atmospheric Simulation
11 Chambers.

12 * *Corresponding author:* Federico Mazzei; federico.mazzei@ge.infn.it

13
14 **Abstracts**

15 Biological Particulate Matter or bioaerosol are a subset of atmospheric aerosol. They influence
16 climate, air quality and health via several mechanisms which often are poorly understood. In
17 particular, the quantitative study of possible relationship between bioaerosol viability and air
18 quality or meteorological conditions is an open and relevant issue. The difficulty of retrieving such
19 possible correlations by analyses of data collected during in-field campaigns, can benefit of
20 targeted experiments conducted in well controlled conditions inside Atmospheric Simulation
21 Chambers, ASCs. ChAMBRe (Chamber for Aerosol Modelling and Bio-aerosol Research) is an
22 ASC in Genoa (Italy) designed and built to perform experimental research on bioaerosol. In this
23 article we focus on bacteria viability. A multi-step protocol was developed and thoroughly tested:
24 cultivation of a suitable bacteria population (*E. coli*), nebulization and injection in the chamber of
25 viable cells, exposure and monitoring of the viability variation inside ChAMBRe, hold at selected
26 conditions, and finally incubation and counting of the concentration of viable bacteria. The whole
27 procedure showed an estimated life time of total (T) and viable (V) *E.coli* of about 153 and 32
28 minutes, respectively, and a V:T ratio lifetime of 40 ± 5 minutes-a reproducibility at the 20% level
29 when ChAMBRe is held kept in a reference “baseline” condition. The coefficient of variation of
30 13% is figure-shows how sensitive quantifies the protocol is also sensitivity as well to changes in
31 viability when the bacteria are exposed to in other (e.g., polluted) conditions. First results showing

32 a viability reduction observed exposing the *E. coli* strain to NO_x concentrations and solar
33 irradiation are presented and discussed. Present results pave the way to systematic studies aimed
34 at the definition of dose-effect relationship for several bacteria strain at atmospheric pollutants.

35

36 **1. Introduction**

37 This article focusses on *bioaerosol*, the aerosol of biological origin. The major types of bioaerosols
38 are primary and secondary biological aerosols and biogenic aerosols.

39 Primary biological aerosols (PBAs) refer to bioaerosols that are directly released into the
40 atmosphere from biological sources, such as plants, animals, or microorganisms; these aerosols
41 can be composed of various biological materials, including bacteria, viruses, fungi, pollen, spores,
42 algae, or other organic particles (Ariya and Amyot, 2004; Fröhlich-Nowoisky et al., 2016).

43 Secondary biological aerosols (SBA) are the result of environmental processes or human activities
44 that modify or transform primary biological aerosols. Unlike primary biological aerosols, SBA are
45 not directly released from biological sources but are generated through secondary processes, like
46 oxidation, condensation, etc., involving biological materials. SBA are fragments of larger
47 biological particles, material released from cells (disruption, excretion...), nucleated biogenic
48 gases, or cells “born” in the air from microbial multiplication Examples of these SBA are dimethyl
49 sulfide and other volatile organic carbons such as methane (Morris et al., 2014, Ervens et Amato,
50 2020 Morris et al., 2014).

51 The PBAs ~~can~~ vary in size depending on the specific biological material being aerosolized; they
52 ~~can~~ range from several nanometers (e.g., viruses, cell fragments) to a few hundred micrometers in
53 aerodynamic diameter (e.g., pollen, plant debris) (Pöschl, 2005). Larger particles of biological
54 material, such as large pollen grains or larger fragments of plants or insects, can be lifted into the
55 air; however, due to their relatively high settling velocities, they tend to rapidly settle or deposit
56 onto surfaces rather than remain suspended in the air for extended periods. As a result, these larger
57 particles are typically not considered atmospheric aerosol particles (Després et al., 2012).

58 Among all the different bioaerosol microorganisms, bacteria are considered to play a significant
59 role in the composition and dynamics of bioaerosols (~~Bowers et al., 2011~~ Gong et al., 2020). They
60 are ubiquitous in the atmosphere, and their presence and abundance can vary depending on factors
61 such as location, season, and local environmental conditions: usually, over the land, the
62 concentration in atmosphere is greater than 10⁴ cells m⁻³ (~~Bauer et al., 2002~~ Burrows et al., 2009)

63 while our understanding of airborne microbes over oceans, is indeed limited compared to the
64 knowledge we have about microbes in terrestrial and aquatic environments. In a recent work
65 (Mayol et al., 2014), the airborne prokaryotic abundance over the North Atlantic ocean ranged
66 from about 3000 to 20000 prokaryotes m⁻³ (average about 8000 cells m⁻³) ~~over the sea, it tends to~~
67 ~~be lower, usually by a factor of about 100 to 1,000. This lower concentration is primarily attributed~~
68 ~~to the relatively cleaner marine environment and the reduced availability of bacterial sources~~
69 ~~compared to terrestrial environments (Prospero et al., 2005; Griffin et al., 2006);~~

70 Bacteria, as small airborne particles or aerosols can have relatively long atmospheric residence
71 times compared to larger particles. This is due to their small size and low settling velocity, which
72 allows them to remain suspended in the air for prolonged periods. ~~Bacteria have a relatively long~~
73 ~~atmospheric residence time, of the order of several days or more, compared to larger particles and~~
74 ~~can be transported over long distances, up to thousands of km~~ (Després et al., 2012). Airborne
75 bacteria may be suspended as individual cells or attached to other particles, such as soil or leaf
76 fragments, or found as agglomerates of many bacterial cells (Lighthart, ~~2006~~1993). For this reason,
77 whereas individual bacteria are typically on the order of ~1 µm or less in size, the median
78 aerodynamic diameter of particles containing culturable bacteria at several continental sites has
79 been reported to be ~ 2 - 4 µm (Shaffer and Lighthart, 1997; ~~Tong and Lighthart, 1999~~; Wang et
80 al., 2007).

81 Even if up to now several works have contributed to the identification of bacterial diversity in the
82 atmosphere (Amato et al., 2007; Burrows et al., 2009; Després et al., 2012, Romano et al., 2019),
83 it remains difficult to establish a clear picture of the actual abundance and composition of bacteria
84 in the air.

85 Numerous studies have suggested that the presence of bacteria in the atmosphere can have
86 significant implications for cloud formation, atmospheric chemistry, microbial biogeography, and
87 climate. As a matter of fact, bacteria can serve as ice nucleating particles and cloud condensation
88 nuclei, influencing the precipitation processes, affecting cloud lifetime, optical properties, and
89 climate patterns (Bauer et al., 2003; Morris et al., 2004; Sun and Ariya, 2006; Möhler et al., 2007).

90 In particular, bacterial viability, the proportion of viable to total bacteria concentration, can act as
91 Cloud Condensation Nuclei (CCN) thanks to the hygroscopic properties of their surfaces (Delort
92 et al., 2010). Additionally, the near-surface atmosphere's viable bacteria can have a significant

93 impact on human health, including allergies, acute toxic effects, and infections (Bolashikov and
94 Melikov 2009).

95 Since bacteria have also been shown to metabolize within cloud droplets, some authors have
96 proposed an impact on the chemistry of cloud droplets and air (Fankhauser et al., 2019 ; Jaber et
97 al., 2021, 2020 ; Khaled et al., 2021 Ariya et al., 2002; Ariya and Amyot, 2004; Amato et al., 2005,
98 2006, 2007; Deguillaume et al., 2008). Finally, the presence of bacteria in the atmosphere can
99 influence microbial biogeography (Martiny et al., 2006) by facilitating long-distance dispersal and
100 the establishment of microbial populations in new environments.

101 Bacteria can enter the atmosphere as aerosol particles from various surfaces, including soil, water,
102 and plant surfaces (Burrows et al., 2009). Once in the air, they are carried upwards by air currents
103 and may remain in the atmosphere for many days before being removed by wet or dry precipitation
104 or direct deposition onto surfaces. Indeed, the mechanisms that govern the transport, survival, and
105 activity of bacteria in the atmosphere are complex and multifaceted. Understanding these
106 mechanisms is crucial for various scientific disciplines, including microbiology, atmospheric
107 science, and public health. This complexity is related to some key factors such as aerosolization,
108 transport and dispersion, survival, hygroscopicity, interactions with other particles, droplet
109 nucleation, deposition, activation of ice nucleation, impacts on cloud formation and chemistry and
110 all these processes are indeed intertwined (Amato et al., 2023).-The interactions between bacteria
111 and their living environment, as well as the atmospheric conditions, play crucial roles in
112 determining their behavior and impacts on climate (Deguillaume et al., 2008) and, consequently,
113 on health.

114 Atmospheric Simulation Chambers (ASCs) have been widely used to study chemical and
115 photochemical atmospheric processes, but the high versatility of these facilities allows for a wider
116 application covering all fields of atmospheric aerosol science. For example, a consistent
117 improvement in characterizing bioaerosols, in understanding the mechanisms affecting their
118 behavior in the atmosphere and finally in elucidating their impacts, can be obtained using
119 atmospheric chamber facilities, where transdisciplinary studies addressing- gathering-atmospheric
120 physics, chemistry, and biology issues are possible.

121 In the last decades, the use of atmospheric simulation chambers has been much more focused on
122 the potential interest of bioaerosol as ice nuclei and cloud condensation activity (Möhler et al.,
123 2008b; Bundke et al., 2010; Chou, 2011). Few studies have investigated bacterial survival and

124 [activity using simulation chambers, and some of them are old \(Wright et al., 1969 Ehrlich et al.,](#)
125 [1970; Krumins et al., 2014; Wright et al., 1969\).](#) Recently, addressing the public health concerns
126 related to bioaerosol contamination has led to increased research efforts focusing on the survival
127 and transformation of bioaerosols in the atmospheric environment. Innovative chamber studies
128 have been initiated to investigate these questions and gain insights into the behavior of bioaerosols
129 (Amato et al, 2015; Brotto et al, 2015). These works have led to the development of a new
130 dedicated simulation chamber, ChAMBRé (Massabò et al., 2018). The chamber has been installed
131 at the National Institute of Nuclear Physics in Genoa (IT) in collaboration with the Environmental
132 Physics Laboratory at the Physics Department of the University of Genoa. ChAMBRé is also a
133 National Facility of the constituting ERIC-ACTRIS, the worldwide largest research infrastructure
134 to study atmospheric phenomena, set up by the European Union on April 25th 2023 (CID, 2023).
135 The main scientific target at ChAMBRé, is the description of biological micro-organisms behavior
136 in the atmosphere, aiming to a deeper understanding of the still unclear mechanisms that control
137 the evolution of bioaerosols in atmosphere, in particular their bacterial components. The long-term
138 goal is the parameterization of survival and activity of bioaerosols to develop specific tools to be
139 implemented in chemical transport models (e.g., CAMx, Wagstrom et al., 2008) presently limited
140 to treat transport and chemistry of gaseous and not-biological aerosol species.
141 This article gives all the details of the present status and capability of the ChAMBRé facility and
142 introduces a multi-step, interdisciplinary procedure assessed to perform quantitative studies on the
143 impact of different pollutants on bacteria viability. Preliminary results are also shown to illustrate
144 the sensitivity of the experimental procedures developed at ChAMBRé that pave the road to
145 systematic investigations on different strains and air quality conditions.

146

147 **2. Material and Methods**

148 Since the beginning of 2017, ChAMBRé has been one of the nodes of the EUROCHAMP-2020
149 network with specific tasks on bio-aerosol studies. From the date of installation on, ChAMBRé
150 control and acquisition system has been enriched with a wide range of equipment aimed at
151 monitoring and controlling the processes occurring inside the chamber. In addition, most efforts
152 have been devoted to developing protocols to produce, inject, expose and collect bio-aerosols, to
153 maximize the experiments reproducibility.

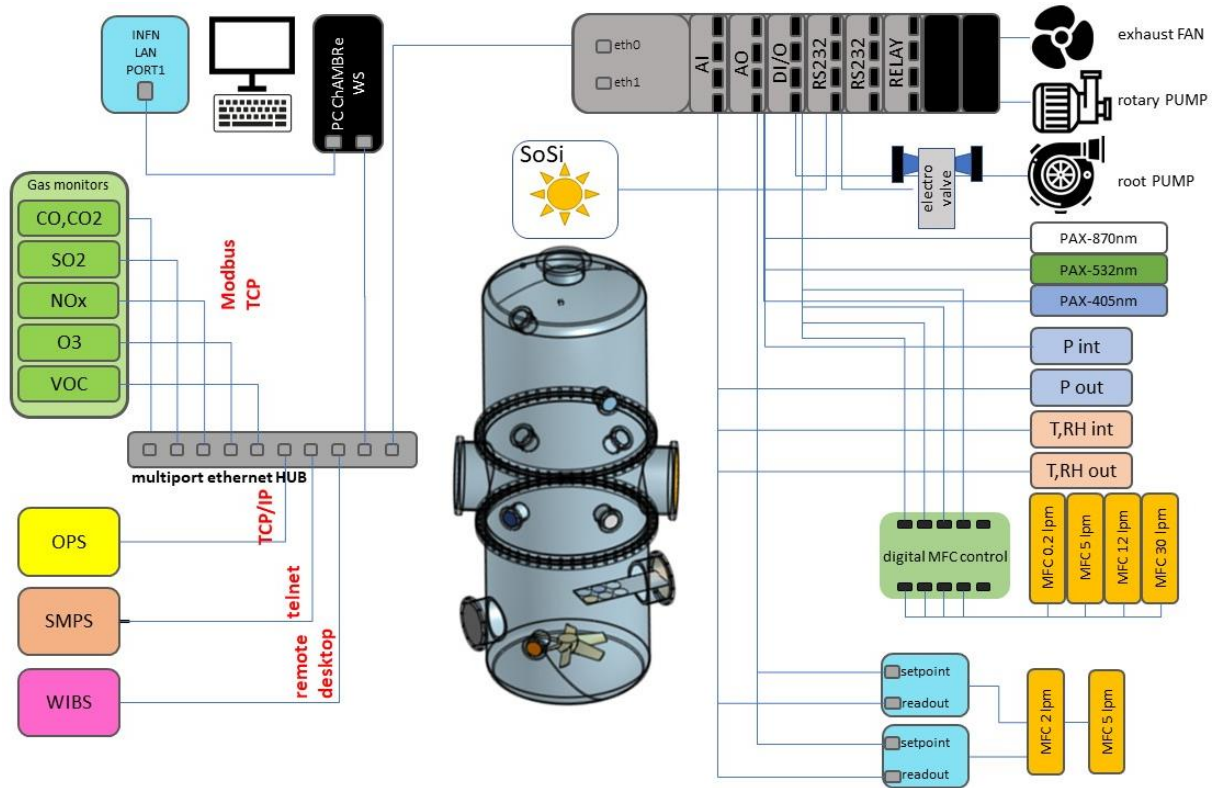


Figure 1: ChAMBRe layout

154
 155
 156
 157
 158
 159
 160
 161
 162
 163
 164
 165
 166
 167
 168
 169
 170
 171

Briefly, ChAMBRe (Massabò et al., 2018) has a cylindrical shape with domed bases. It has a maximum height and diameter of 2.9 and 1 m, respectively, and a total volume of about 2.2 m³. The main body is divided into three parts (two domed cylinders connected by a central ring) equipped with several flanged apertures of different diameters matching the different types of fitting for instrument interfacing. To favor the mixing of the gas and aerosol species, a fan is installed at the bottom of the chamber. It is a standard venting system with a particular pass-through designed and built at INFN-Genoa to ensure the vacuum seal. The fan speed can be regulated by an external controller and set up to 50 Hz in steps of 0.1 Hz. One of the two flanges in the bottom part is connected through a pneumatic valve to a smaller horizontal cylinder (length about 1 m), which hosts a movable tray designed to move specific samples inside the chamber. The samples are typically Petri-dishes for bacteria collection inside the chamber during the experiments: they can remain exposed for the whole experiment or for a selected time interval controlled by the user. A custom-made side flange has been worked in the central ring of the main body of the chamber. The large tipper tailgate allows the introduction and

172 positioning of bulky sensor devices for testing and calibration purposes. The flange features a
173 small window for visual inspection and four vacuum feedthrough connectors to power and
174 communicate with devices inserted in the chamber.

175 ChAMBRé is equipped with a composite pumping system (rotary, root and turbo pump) which
176 can evacuate the internal volume to a level of about 5×10^{-4} mbar. The return to atmospheric
177 pressure can proceed by flowing ambient air inside the chamber through a five-stage
178 filtering/purifying/drying inlet system including an absolute HEPA filter and a zeolite trap or using
179 synthetic air from a cylinder (reducing the relative humidity close to zero).

180 Two types of UV lamps are permanently installed inside the chamber. A 58 cm long lamp ($W =$
181 60 W , $\lambda = 253.7 \text{ nm}$; UV-STYLO-F-60H, Light Progress Srl) is inserted through a custom side
182 flange to sterilize the chamber volume without producing ozone after any experiment involving
183 bioaerosol. A second type of lamp, producing UV radiation at $\lambda < 240 \text{ nm}$, can be inserted through
184 one of the ISOK100 flanges of the central ring to generate ozone.

185 A set of two pressure gauges is used to measure the atmospheric pressure inside (range $5 \times 10^{-4} -$
186 10^3 mbar) and outside (range of $5 \times 10^{-2} - 10^3 \text{ mbar}$). ChAMBRé internal temperature and relative
187 humidity are continuously measured by a sensor located in the upper ISO-K100 flange on the top
188 dome.

189 Supervised injection of known volumes of different gas species inside the chamber is made by a
190 set of software-controlled digital mass flow controllers (MFC) ranging from 5 to 30 lpm full-scale
191 manufactured by Bronkhorst[®]. ~~Two 5-lpm MFCs are dedicated to the injection of CO₂ and SO₂~~
192 ~~whose concentration inside the chamber can be selected by the operator (ppm or ppb units) and~~
193 ~~kept constant during the experiment thanks to a PID (Proportional-Integral-Derivative) controller~~
194 ~~algorithm. Two 5-lpm MFCs are designed for injection of CO₂ and other gases (i.e. SO₂, CO, NO~~
195 ~~and NO₂), respectively, whose concentration in the chamber can be selected by the operator (ppm~~
196 ~~or ppb units); a PID (Proportional-Integral-Derivative) controller, using the gas concentration~~
197 ~~values read from the corresponding gas analyzer, keeps the gas concentration in ChAMBRé~~
198 ~~constant during the experiment.~~

199 A 30-lpm MFC regulates the injection of dry air inside the chamber. In this case, the PID controller
200 ~~(using the ChAMBRé pressure values measured by pressure sensor mentioned above)~~ allows to
201 maintain a pre-defined pressure gap between inside and outside the chamber. A 12-lpm and a 0.2-
202 lpm MFCs are dedicated to the injection of known volumes of air and fuel, respectively, inside the

203 burning chamber of a Mini Inverted Soot Generator MISG ~~soot generator device~~ (Argonaut
204 Scientific Corp., Edmonton, 49 AB, Canada, Model MISG-2). The MISG can be connected to an
205 inlet flange of ChAMBRé for the study of the properties of soot particles exposed and maintained
206 in different conditions or to study the effects of soot particles. The input air flow of the nebulizers
207 (see Par. 2.2), responsible for the crucial process of bacteria injection inside the chamber, is
208 regulated by an analog 5-lpm full-scale MFC (EL-Flow[®]) ~~connected to the nebulizer inlet.~~

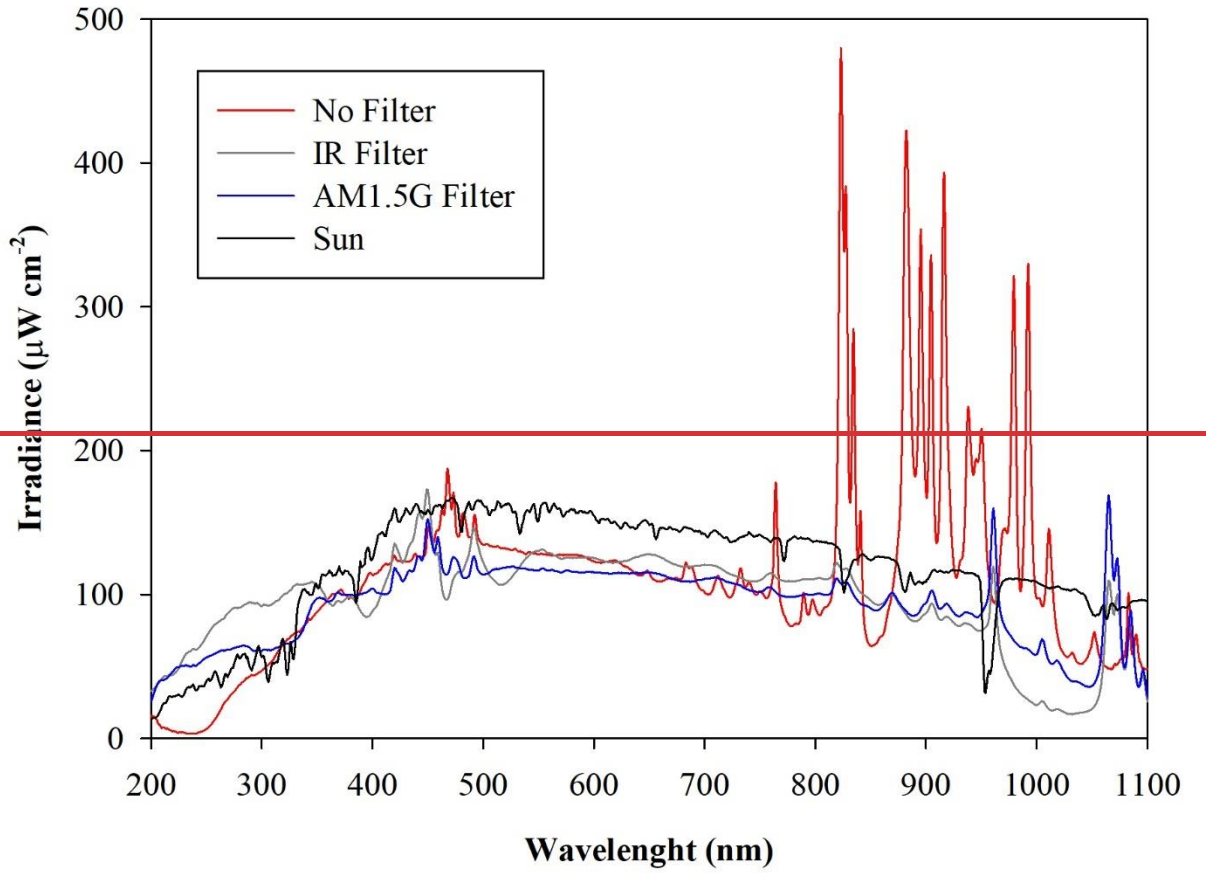
209

210 *2.1 Instruments permanently connected to the chamber.*

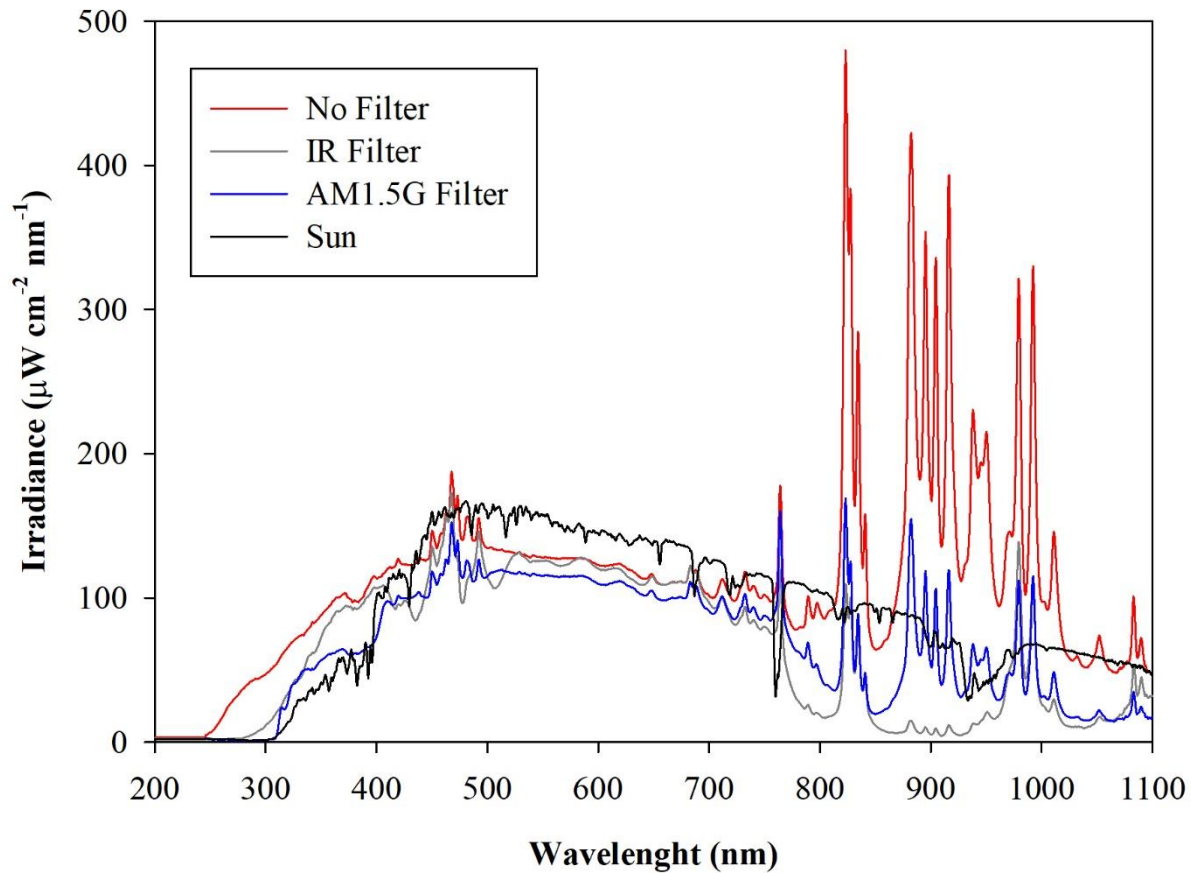
211 The concentration of several gaseous pollutants potentially present inside the chamber (~~or in the~~
212 ~~laboratory~~) can be monitored by a set of calibrated gas detectors manufactured by ENVEA[®]: non-
213 dispersive Carbon monoxide and dioxide analyzer (CO12e), Ozone analyzer (O342e), Sulfur
214 dioxide analyzer (AF22e), chemiluminescent Nitrogen Oxides analyzer (AC32e) and Gas
215 chromatography VOC analyzer (VOC72M). Details on the quoted monitors are provided in
216 Supplement S1.

217 A custom solar simulator manufactured by Sciencetech[™] has been installed on the top of the upper
218 dome of the chamber. The top ISO-K250 flanged aperture has been appropriately modified by
219 inserting a dedicated quartz window (diameter = 25 cm) with a high degree of transmittance (> 95
220 %, with $300 < \lambda < 900$ nm) and reflectance (< 1.5% with $300 < \lambda < 900$ nm) to the solar spectrum
221 radiation. The system consists of two main sections: the light source and the power supply. The
222 light source, a 1600 W Xenon Short Arc lamp (Sciencetech[™] - XE1600), is mounted inside a
223 dedicated housing where a set of optical lenses and mirrors deflects the light beam perpendicularly
224 to fit the quartz window aperture. A set of filters are available to intercept the light beam and cut-
225 off selectable portions of the spectrum before entering the chamber. In particular, the simulator
226 can be fitted with a low-pass optical filter, designed to cut off a portion of the spectrum in the
227 infrared (IR) region. Alternatively, the optical absorption of the atmosphere can be simulated by
228 using a dedicated filter (AM1.5G 3 × 3" air mass filter, Sciencetech[™]), which cuts off selected
229 bands to mimic the light interaction of an air mass coefficient of 1.5 (i.e., an optical path length
230 that is 1.5 times that of light traversing the atmosphere at the zenith). Figure 1 shows the impact
231 of the available filters on the light spectrum sent to the chamber. The nominal maximum irradiance
232 provided by the Solar Simulator without any filter is about 2.4 SUN, actually 2,424 W m⁻²,

233 corresponding to about 119 W passing through the quartz window on the ChAMBRé top dome
234 with the AM1.5 filter mounted inside the solar simulator.
235



236

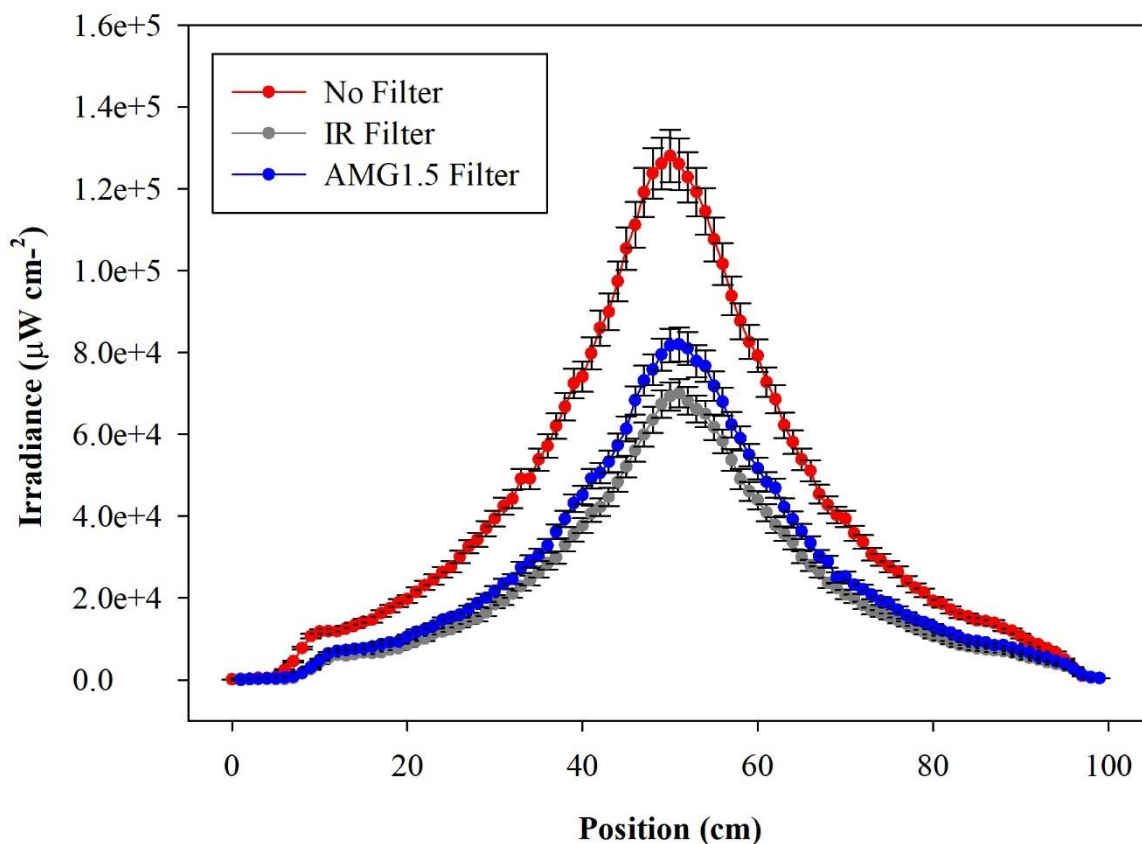


237
 238 **Figure 2:** Irradiance vs wavelength measured with a calibrated Avantes ULS2048CL-EVO spectrometer directly at
 239 the exit of the Solar Simulator with and without the available filters. The spectrum labelled “Sun” has been measured
 240 on a springtime sunny day in the terrace of the Physics Department in Genoa, Italy. The uncertainties of irradiance
 241 (not reported in the graph) are $\pm 10\%$ from 200 to 350 nm and 5% from 350 to 1100 nm

242
 243 The solar simulator is also equipped with a set of four neutral density optical filters, to reduce the
 244 light intensity entering the chamber. These filters provide an attenuation of 19%, 34%, 50% and
 245 71% of the lamp power, respectively, and can be fitted two at a time on the device, offering a
 246 minimum transmittance of 7%. The neutral density filters do not significantly alter the shape of
 247 spectrum of the transmitted light, attenuating the optical power uniformly (see Supplement S2,
 248 Figure S2).

249 The radial distribution of the optical power measured inside the chamber volume is shown in
 250 Figure 3, as a function of the distance along a cross-sectional diameter in the center of ChAMBRé.
 251 The light intensity has a strong peak at the center of the diameter, where the optical power is more

252 than six times that close to the walls. To obtain the total light intensity irradiated by the lamp in
 253 the chamber volume, the measured data points were fitted with a double gaussian function, which
 254 was then integrated in cylindrical coordinates, exploiting the symmetry of the light beam. The
 255 resulting intensity is 160 ± 6 W with the lamp set at full power (power supply set at 105% of the
 256 nominal value) and no optical filter. The total intensity with the AM1.5 filter is 94 ± 4 W, while
 257 with the IR filter the total integrated intensity is 81 ± 4 W. With respect to the irradiance measured
 258 directly at the Solar Simulator output, the value inside the chamber shows just a loss of about 20%
 259 (likely due focusing/collimation). It must be noted that, at the maximum power and no-filter, the
 260 irradiance measured on the middle plane of ChAMBRe is about 0.2 SUN, this almost
 261 corresponding to the dilution given by the ratio of the surfaces of the top quartz window (diameter
 262 of 25 cm) and of the chamber (diameter of 100 cm).



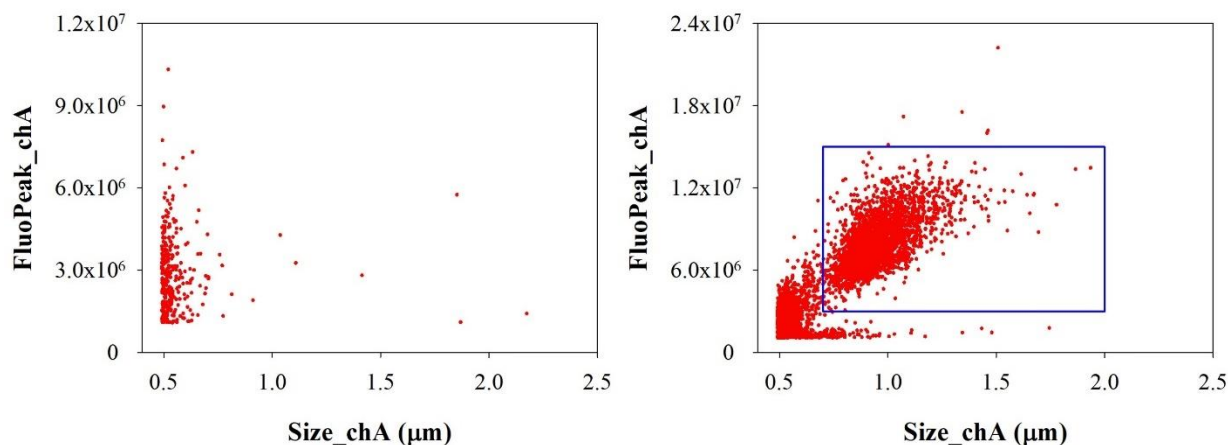
263
 264 **Figure 3:** Irradiance vs wavelength measured with a calibrated Avantes ULS2048CL-EVO spectrometer along a
 265 diameter at the center of the ChAMBRe volume, with and without the available optical filters. The center of the
 266 chamber is at position=50 cm.

267 Particle concentration and size distribution inside ChAMBRe are real-time monitored by a
268 Scanning Mobility Particle Sizer (SMPS; TSI Inc., model 3938), in the range of 10 – 1000 nm,
269 and an Optical Particle Sizer (OPS; TSI Inc.; model 3330) in the range 0.3 - 10 μm .
270 The SMPS is formed by three components: a neutralizer (i.e., a bipolar diffusion charger), a
271 differential mobility analyzer (DMA, series 3080) and a condensation particle counter (W-CPC,
272 model 3789), from TSI Inc. The model 3088 Neutralizer uses a low-energy ($< 9.5\text{keV}$) soft X-ray
273 source to generate high concentrations of both positive and negative ions to bring the aerosol to a
274 defined, steady-state charge distribution. The DMA is available with two different columns: model
275 3081 Long DMA, which provides the widest size range of 10-1000 nm, and the model 3085 Nano
276 DMA, which covers the range of particle diameter from 2 and 150 nm. In a DMA, an electric field
277 is created and the airborne particles drift in the DMA according to their electrical mobility. Particle
278 size is then calculated from the mobility distribution. In the CPC, downstream of the DMA, the
279 particle size is increased by water condensation on their surface and then the particles are optically
280 counted. The maximum measurable concentration can reach 2×10^5 particles cm^{-3} . The SMPS
281 working airflow ranges between 0.2 and 1.5 lpm.

282 The Model 3330 OPS is an optical particle sizer spectrometer that provides measurement of
283 particle number concentration and particle size distribution based on single particle counting
284 technology. The OPS has an inlet flow rate of $1.0 \text{ lpm} \pm 5\%$ and measures particles from 0.3 μm
285 to 10 μm in 16 user-adjustable size channels (particles above 10 μm are counted but not sized).
286 The OPS 3330 works on the principle of optical scattering from single particles. The OPS uses a
287 laser beam ($\lambda = 660 \text{ nm}$) and a detector to detect particles passing through a sensing volume
288 illuminated by the laser. Particle pulses are counted individually and binned into 16 channels up
289 to their pulse heights. The OPS is factory calibrated using different monodispersed Polystyrene
290 Latex particles (PSL) for size classification; size resolution is 5% at 0.5 μm following the
291 procedure described in the ISO 21501-1 normative. Particles exiting the chamber are trapped by a
292 gravimetric filter for possible after sampling chemical analysis.

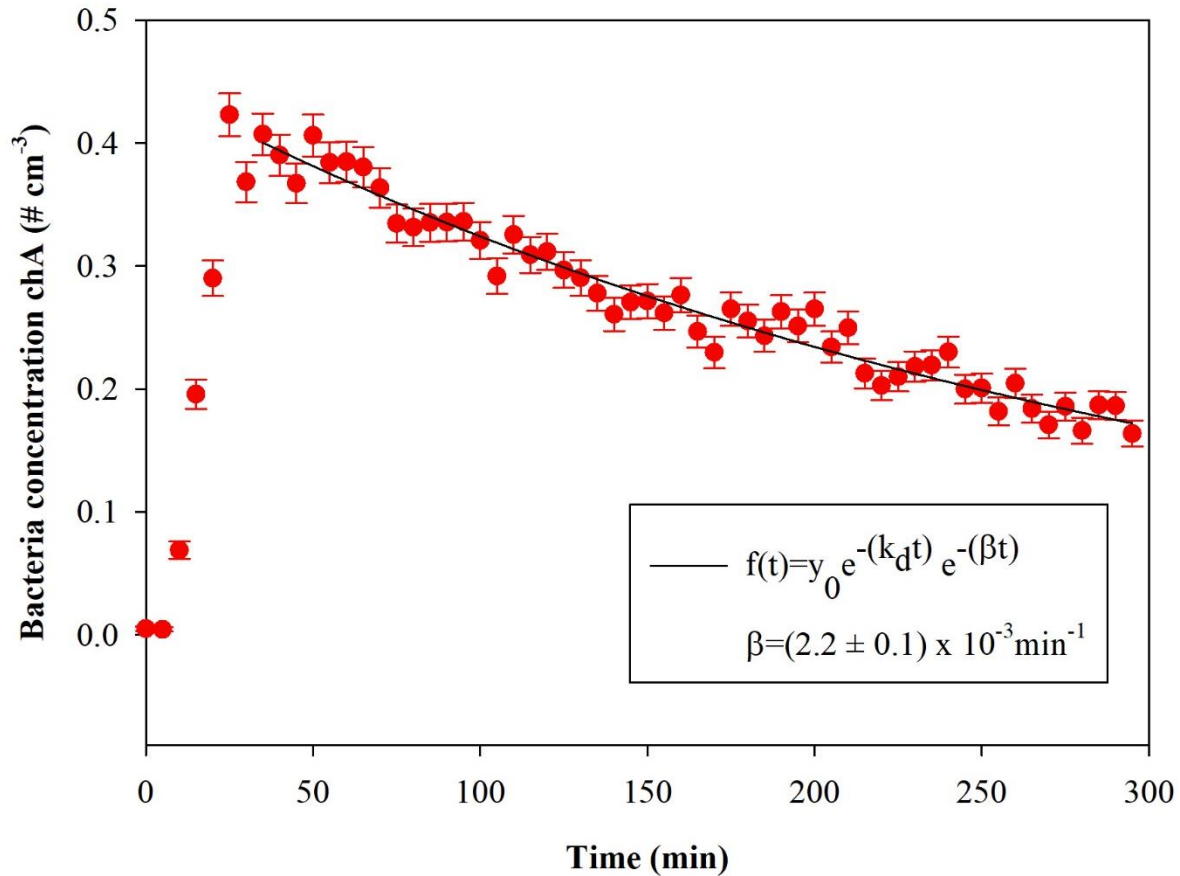
293 A Waveband Integrated Bioaerosol Sensor (WIBS-NEO, Droplet Measurement Technologies[®])
294 has been integrated in the ChAMBRe particle monitoring system to measure bio-aerosols
295 concentration. The instrument uses two UV filtered flashlamp sources ($\lambda = 280 \text{ nm}$ and $\lambda = 370$
296 nm) to excite fluorescence in individual particles (Lieberherr et al., 2019). Detection wavebands

297 have been selected to optimize detection of common bioaerosol components and let the user
298 discriminate between different types of biological micro-organisms (bacteria, fungi, pollen, etc.).
299 The massive amount of data generated by the WIBS during the experiments at ChAMBRé through
300 a list-mode off-line analysis, has made necessary to develop a dedicated software tool, written in
301 Igor 8.0 (Wavemetrics, Inc.) language, aimed at implementing a multi-parametric data reduction
302 and to retrieve the airborne bacteria/bioaerosol concentration inside the chamber as a function of
303 time. Starting from the raw data, the Igor procedure first sets a background threshold for the
304 particle fluorescence intensity and groups the particles into three channels (A, B, C) and their
305 relative intersections (AB, AC, BC, ABC) according to their presence within the three fluorescence
306 detection waveband groups (FL1, FL2, FL3), following the terminology adopted in the WIBS
307 (Lieberherr et al., 2019). Then, for signal-background separation purpose, fiducial cuts are applied
308 on scatter plots (Fluorescence Intensity vs Particle Size) relative to particles belonging to channel
309 A, which is known to be mainly populated by particles showing a bacteria-like fluorescence
310 emission. Examples of the scatter plots are reported in Figure 4 where the region of interest of the
311 signal (*E. coli* bacteria) is well separated from the background region.



312
313 **Fig 4:** Size distribution of particles in channel A. Left: background measured without any bacteria injected in
314 ChAMBRé. Right: particles population after *E. coli* injection. The particles inside the blue rectangular region of
315 interest are identified as *E. coli*.

316
317 Finally, the whole analysis is cycled over user-selectable time intervals to retrieve the time-
318 resolved particle concentration during the whole experiment. Figure 5 shows the time series of *E.*
319 *coli* concentration inside the chamber during a typical experiment.



320
 321 **Figure 5:** Temporal trend of *E. coli* particles inside the chamber; $t = 0$ is the injection start. The curve fit is also shown,
 322 where β is the particle loss rate coefficient and k_d is the dilution factor (here $k_d = 1.02 \times 10^{-3} \text{ min}^{-1}$). The error bars are
 323 the standard deviations calculated following the Poisson statistics.

324
 325 Optical properties (i.e., absorption, extinction and scattering coefficients) of particles suspended
 326 inside the chamber can be measured online by photoacoustic extinction meters (PAXs; Droplet
 327 Measurement Technologies) at three wavelengths: $\lambda = 870, 532$ and 405 nm .
 328 The PAX directly measures in-situ light absorption and scattering of aerosol particles, from which
 329 it derives extinction, single scattering albedo and black carbon mass concentration (Vernocchi et
 330 al., 2022). PAX uses a modulated diode laser to simultaneously measure light scattering and
 331 absorption. The standard infrared, 870 nm wavelength option, is highly specific to black carbon
 332 particles, since there is relatively little absorption from gases and non-BC aerosol species at this
 333 wavelength. A nominal 1 lpm aerosol sample flow is drawn into the PAX using an internal vacuum
 334 pump controlled by two critical orifices. The flow is split between the two distinct measurement
 335 regions: a nephelometer, for the light scattering measurement and a photoacoustic resonator for

336 the absorption measurement. Absorbing particles heat up and quickly transfer heat to the
337 surrounding air. A sensitive microphone detects the pressure waves produced by the heating,
338 whose intensities are interpreted to infer the particle absorption coefficient (Moosmüller et al.,
339 2009). In the nephelometer, a photodiode set at 90° with respect to the beam detects the radiation
340 reflected by the sampled particles. The scattering measurement responds to all particle types
341 regardless of chemical makeup, mixing state, or morphology.

342 Acquisition and control of the instruments connected to ChAMBRé is handled by a National
343 Instruments™ based system made up of a main controller (NI9057 cRIO) and several modules (C
344 Series modules), which allow communication with the peripheral devices via analog, serial, and
345 ethernet data transfer protocols. The operator interaction with the sensor network is demanded to
346 a single NI-LabVIEW™ SCADA (Supervisory Control And Data Acquisition) custom application
347 which provides the user with a global data overview and a full real-time control above all the
348 instruments parameters via a user-friendly human-machine interface (HMI). In Supplement S1
349 (Figure S1), a screenshot of the main panel of the SCADA application is shown.

350

351 *2.2 Other equipment for specific applications/experiments*

352 Aerosols to be used in ChAMBRé experiments can be generated in different ways, depending on
353 the specific application. The Flow-Focusing Monodisperse Aerosol Generator (FMAG, TSI Inc.
354 model 1520) can be used to produce monodisperse particles in the diameter range 0.8 - 12 µm,
355 starting from both liquid and solid materials. The ~~Mini-Inverted-Soot Generator (MISG; Argonaut~~
356 ~~Scientific Corp., model MISG-2)~~ is used to produce soot particles from the controlled combustion
357 of different gaseous fuels (Vernocchi et. al 2022).

358 Three nebulizers, designed for bioaerosol applications, are also available: the Collison nebulizer,
359 the Blaustein Atomizing Modules (BLAM), and the Sparging Liquid Aerosol Generator (SLAG),
360 all manufactured and distributed by CH TECHNOLOGIES Inc. The performances of the three
361 nebulizers in connection to the injection of viable bacteria in the chamber have been previously
362 investigated and described in (Danelli et al., 2021).

363 Bacteria injected inside ChAMBRé can be collected by different methods. All the methods
364 described below allow to perform offline analyses. A cylindrical horizontal volume is connected
365 to the chamber by an ISO-KF250 pneumatic valve; this volume can be alternatively opened or
366 closed without perturbing the inner atmosphere thanks to another ISO-KF250 pneumatic valve.

367 Inside the cylinder, there is a sliding tray that can be inserted in ChAMBRé by an external manual
368 control, to minimize the risk of contamination. The tray can host up to six Petri dishes (diameter
369 10 cm, each) to collect bacteria (or in general BPA) directly by gravitational settling. In addition,
370 bacteria can be collected on solid medium (i.e., Petri dishes filled with culture medium) by the
371 active sampling by an Andersen impactor (Single Stage Andersen Cascade Impactor, TISCH
372 Environmental) working at a fixed air flow of 28.3 lpm, supplied by a dedicated pump. The
373 impactor is connected to the chamber by ISO-K flanges. Moreover, bioaerosol can be collected
374 through liquid impinger, (Flow Impinger, Aquaria srl), filled with 20 ml of sterile liquid solution,
375 ~~allowing subsequent offline laboratory analysis~~. Such a device can be easily connected to the
376 chamber volume through the ISO-K flanges. Impinger operates at a constant airflow of 12.5 lpm
377 (e.g., by a low-capacity pump: Model LCP5, Copley Scientific). Finally, aerosol suspended in the
378 chamber can be also collected on filters (i.e., quartz fibre, PTFE, cellulose) ~~for offline analysis~~.
379 Sampling is managed by a low-volume particulate matter sampler, setting the air flow in the range
380 10 – 50 lpm.

381

382 2.3. *Equipment to manipulate bioaerosol*

383 A biological laboratory with specific instrumentation for isolating and maintaining bacterial cells
384 culture is part of the ChAMBRé facility:

- 385 • Biosafety cabinet, and laminar flow hood, Miniflow Linear blue air Aquaria, (Milano,
386 Italy). It is used to provide a contamination-free working environment for the workers. A
387 laminar flow filters the air and traps dust particles and microbes for providing a sterile
388 working environment in the stainless-steel cabinet. The hood is equipped with HEPA filter
389 and an UV-light lamp allows the sterilization of the illuminated surfaces inside the hood.
390 ~~laminar is created inside the cabinet.~~
- 391 • Centrifuge MPW-352 MPW MED Instruments (Warsaw, Poland) used to separate particles
392 from a homogeneous solution through rotational movement and centrifugal acceleration,
393 causing sedimentation of its components. The MPW-352 has a swinging-bucket rotor that
394 swings out when centripetal force is applied and holds the pellet at an approximate 90°
395 angle relative to the angle of rotation.

- 396 • Spectrophotometer Shimadzu 1900, designed for liquid samples, is a double-beam UV-Vis
397 Shimadzu Corporation, Japan. This instrument measures intensity as a function of light
398 source wavelength. For each wavelength of light passing through the spectrometer, the
399 intensity of the light passing through the sample cell is measured. The biological
400 applications include measurement of substance concentration such as protein, DNA or
401 RNA, growth of bacterial cells, and enzymatic reactions.
- 402 • Shaker incubator, designed for liquid samples, with orbital rotation movement SKI 4
403 ARGOLAB, Carpi MO – Italy. It provides a controlled environment for samples to grow
404 and develop while also providing mechanical agitation to mimic the natural movement of
405 cells in their environment. Shaking can be used to promote the growth and development of
406 cells and microorganisms to increase the oxygen supply to the cells. The oxygen is an
407 important factor that can affect the growth and metabolism of cells. By shaking the culture,
408 it is possible to increase the oxygen supply to the cells by increasing the diffusion of oxygen
409 into the media.
- 410 • ~~Quantom Tx microbial cell counter Logos Biosystems, South Korea. This automated cell~~
411 ~~counter can detect individual bacterial cells in a liquid sample. The instrument provides~~
412 ~~counting of the total number of cells in the suspension using fluorescent probe. It captures~~
413 ~~images of (10-fields) fluorescence-stained cells. The optimal concentration range of count~~
414 ~~is $5 \times 10^5 - 5 \times 10^8$ cells ml⁻¹ and the size range of the count cells is between 0.3 and 50~~
415 ~~µm. To evaluate the uncertainty on the bacteria count (QT x TOT), we repeated the~~
416 ~~measurement on the same sample 10 times, and we found a results repeatability of 5%.~~
417 ~~This uncertainty is much higher than the statistical error of total counting (assuming the~~
418 ~~Poisson statistic), and, for this reason, we adopted a 5% uncertainty to all Quantom Tx~~
419 ~~counts.~~ The sample is prepared from the bacterial suspension in physiological solution
420 immediately before injection; for counting the total number of cells, three different
421 solutions to 10 µl of the initial suspension are added: *Total Cell Staining Dye*, *Total Cell*
422 *Staining Enhancer* and *Loading Buffer I*. The first added is the *Total Cell Staining Dye*, a
423 membrane-permeable fluorescent dye, which is capable of binding to nucleic acids in
424 viable and non-viable cells and allows the detection of Gram-positive and Gram-negative
425 bacteria. This probe has an excitation wavelength of $\lambda = 484$ nm, and it emits $\lambda = 504$ nm.
426 The second solution used is the *Total Cell Staining Enhancer* to guarantee a better cells

427 penetration by the probe and to obtain a uniform background during the images acquisition
428 by Quantom Tx. The sample must be incubated in the dark at 37°C for about 30 minutes
429 to favor the penetration of the fluorescent dye into the cells. Finally, the *Loading Buffer I*
430 is added and used to uniform the distribution and the sedimentation of bacterial cells in the
431 counting stands. The slide, after being centrifuged at 300 RCF for 10 minutes, is inserted
432 in the specific support in the counter and then illuminated with a lamp at $\lambda = 470$ nm with
433 a bandpass of 30 nm. The light power can be set to nine levels of intensity (labelled from
434 1 to 9): in our experiments, the best results are obtained selecting the intensity of 5 for
435 counting total cells.

436 2.3.1 Bacteria cultivation, injection and monitoring

437 The bacteria strain so far used to perform experiments at ChAMBRé is *Escherichia coli* (ATCC®
438 25922™), Gram-negative, purchased by Thermo Scientific™ Culti-Loops™. *E. coli* is rod-shaped,
439 about 1–2 μm long and about 0.25 μm in diameter (Jang et al., 2017). It is a common inhabitant of
440 the gastrointestinal apparatus of warm-blooded animals, including humans. This strain is a non-
441 pathogen proxies of typical atmospheric bacteria, extensively used as model organisms in
442 microbiology and molecular biology fundamental and applied studies (Lee et al., 2002; Lee and
443 Kim, 2003).

444 Bacterial growth is a complex process that involves several distinct phases. The increase in
445 numbers or bacterial mass can be measured as a function of time under culture conditions where
446 the nutrients and environmental conditions are controlled. Several distinct growth phases can be
447 observed within a growth curve such as the lag phase, the exponential or log phase, the stationary
448 phase, and the death phase. The first stage, the lag phase, occurs when bacteria are not dividing
449 but are metabolically active. During the lag phase of the bacterial growth cycle, the synthesis of
450 RNA, enzymes, and other molecules occurs. The length of this phase depends on the type of
451 bacterial species, culture medium, and environmental factors. The log phase is an exponential
452 phase characterized by rapid growth, with binary fission. The number of new bacteria appearing
453 per unit time is proportional to the present population. If growth is not limited, doubling will
454 continue at a constant rate, so both the number of cells and the rate of population increase doubles
455 with each consecutive period. Exponential growth cannot continue indefinitely, however, because
456 the medium is soon depleted of nutrients and enriched with catabolites. (Maier R. et al., 2008).

457 The stationary phase is due to a growth-limiting factor; this is mostly depletion of a nutrient, and/or
458 the formation of inhibitory products such as organic acids. Instead during the death phase, the
459 number of living cells decreases exponentially. Bacteria run out of nutrients and die although the
460 number of cells stays constant. The decline phase is brought by exhaustion of nutrients,
461 accumulation of toxic products, and autolytic enzymes. The microbial growth curve is a record of
462 the countable cells determined at certain time intervals during the population's evolution. In our
463 work, the calibration curve was figured out converting the rate growth from **optical density (OD)**
464 values to CFU (Colony Forming Unit) ml⁻¹, as explained in detail below.

465 The day before the experiment, bacteria cells are scraped off agar medium, where they are
466 cultivated, using sterile plastic loops and suspended in a sterile, non-selective culture broth
467 medium Tryptic Soy Broth (TSB) and incubated overnight at 37 °C. The day after, 3 ml of the
468 bacteria culture is diluted in 30 ml of new broth medium, and the suspension is incubated again at
469 37 °C. At intervals of about thirty minutes, the OD of the bacterial solution is measured by the
470 spectrophotometer at $\lambda = 600$ nm; OD_{600nm} allows to estimate the concentration of bacterial cells
471 in the liquid and tracking the growth. The mid-exponential phase is typically reached when
472 OD_{600nm} is about 0.5 (Mytilinaios et al., 2012; Hall et al., 2014). For selected OD values, the
473 bacterial concentration was also measured/referred as Colony Forming Units (CFU). The bacteria
474 solution must be diluted several times to obtain not overlapping colonies on Petri Dishes: 100 μ l
475 of bacterial solution is added in 900 μ l of sterile saline solution (NaCl 0.9 %), then diluted again
476 as many times as the theoretical concentration (calculated using the OD value) required; 100 μ l of
477 the last dilution is spread in duplicate on an TSB agar and incubated overnight at 37 °C. The next
478 day the concentration of culturable cells is measured by counting the colonies formed and
479 multiplying by the proper dilution factor to retrieve CFU concentration in the original solution.

480 Data, obtained by CFU counting on agar plates, are **weighted** averaged and used to figure out the
481 uncertainty **(standard error of weighted mean)** of the bacterial concentration in the solution
482 **following the Poisson statistics. The weights are the relative uncertainties of CFU number on agar**
483 **plates following the Poisson statistics.**

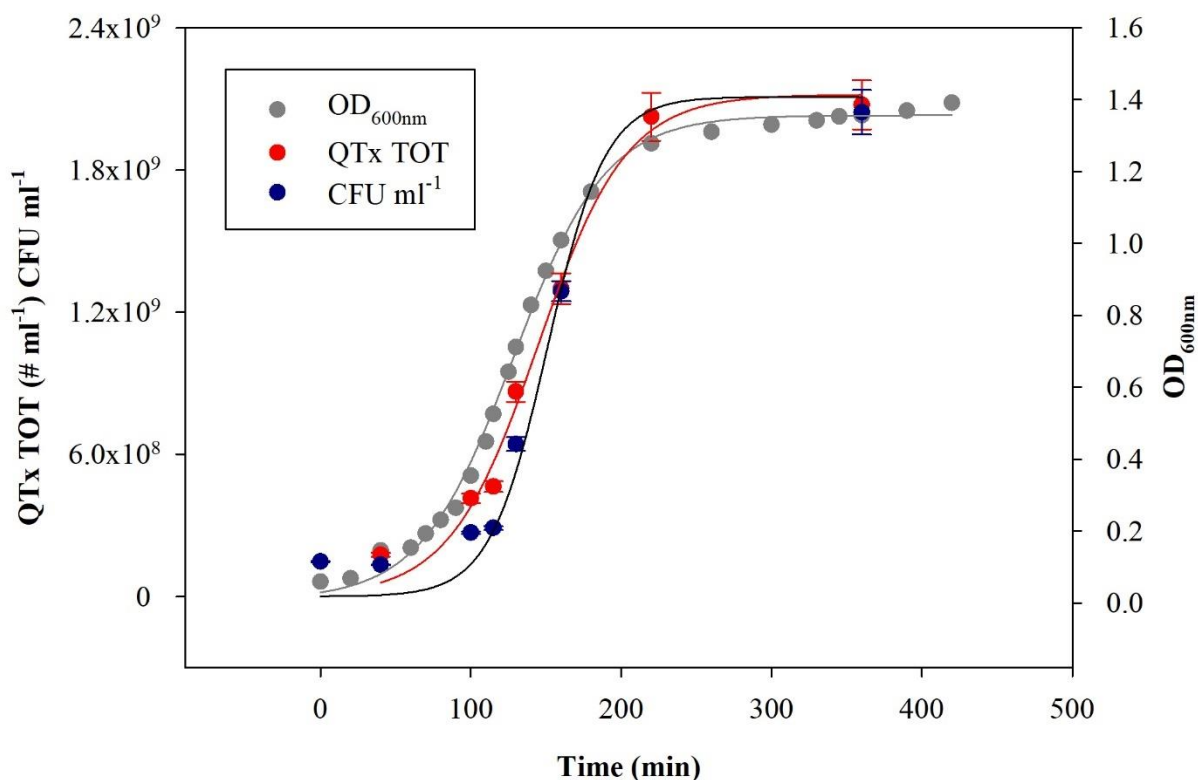
484 Several sigmoidal functions **have were** so far **been** adopted to describe a bacterial growth curve.
485 The literature on these models is well known and is used in various contests: plants, bird growth,
486 fish and other animals, cancers and bacterial growth (Kathleen M. et al., 2017). We tested the fits
487 to our *E. coli* growth curves by Logistic, Gompertz, and Richards models. (Birch C.P. 1999; Baty

488 F. and Delignette-Muller M.L. 2004). The logistic function model is used specifically to describe
 489 growth of microorganisms, as a function of nutrient depletion (Daniel E. W. et al 2003) and it was
 490 demonstrated to be the best fit for modeling bacteria (Akin et al 2020; Annadurai G. et al. 2000).
 491 Here, the results of the logistic fit only are only-shown. The logistic equation was written as:

$$y(t) = \frac{y_0}{1 + e^{-b(t-t_0)}} \quad (1)$$

492
 493
 494 where y indicates the bacteria concentration in the solution, y_0 is the saturation value, b is the
 495 maximum specific growth rate and t_0 is the time at the inflection point.

496
 497 We followed the growth of *E. coli* in suspension culture for about 8 hours from lag phase to
 498 horizontal asymptote and the OD_{600nm} , the total number of *E. coli* (QTx TOT), measured with
 499 Quantum TX and the $CFU\ ml^{-1}$ values are reported in Figure 6. The values of reduced chi-squared,
 500 (χ^2) , y_0 , b and t_0 of the logistic fit for OD_{600nm} , QTx TOT and $CFU\ ml^{-1}$ are reported in Table 1.



501
 502 **Figure 6:** Grow curve for *E. coli*: optical density (OD_{600nm}), total number of *E. coli* measured by QUANTOM-TX (#
 503 ml^{-1}) and the corresponding bacteria concentration ($CFU\ ml^{-1}$) vs. time. Error bars haveare, in most cases, the same
 504 size ofas the data points and they are calculated as previously described.

505

506

Table 1: χ^2 , y_0 , b and t_0 of the logistic fit for OD_{600nm}, QTx TOT and CFU ml⁻¹.

Logistic 3 parameters	OD _{600nm}	QTx TOT (# ml ⁻¹)	CFU ml ⁻¹
χ^2	1.04	1.17	1.17
y_0	1.35 ± 0.01	$(212 \pm 8) \times 10^7$	$(211 \pm 6) \times 10^7$
b (min ⁻¹)	$(3.3 \pm 0.1) \times 10^{-2}$	$(3.4 \pm 0.5) \times 10^{-2}$	$(5.2 \pm 0.4) \times 10^{-2}$
t_0 (min)	128 ± 1	145 ± 5	151 ± 2

507

508 ~~The b values of~~ OD_{600nm} and QTx TOT ~~have the same values of the b parameter~~ are compatible
509 ~~within their uncertainties~~, and this result is expected since the OD_{600nm} is an indirect measurement
510 of the total concentration of cells in suspension. The grow rate of CFU ml⁻¹ is faster and the
511 corresponding doubling time (about 19 minutes) is compatible with the value reported in the
512 literature (Son M.S. et al, 2001).

513

514 2.3.2 Bacteria and experiments in ChAMBRé

515 To prepare the inoculum for the chamber experiments, the *E. coli* is grown in 30 ml of fresh TSB
516 nonselective medium, in a shaking incubator at 37 °C and 200 rpm and its growth is followed by
517 checking the OD_{600nm} value until the mid-exponential phase. When OD_{600nm} ~ 0.5, 20 ml of this
518 liquid preparation ~~the bacteria are~~ centrifugated at 3000 rpm for 10 min. Afterward, ~~the~~ bacteria
519 pellet, separated by supernatant, is ~~are~~ resuspended in 20 ml of sterile physiological solution (NaCl
520 0.9 % w/v) to prepare a suspension of approximately 10⁸ CFU mL⁻¹, as verified by standard
521 dilution plating. To retrieve the bacterial concentration, the average of CFU counting on agar plates
522 and the uncertainty are calculated following the same metric described in 2.3.1 paragraph. ~~and the~~
523 ~~number of cultivable cells is counted as CFU by standard dilution plating on Petri dishes filled~~
524 ~~with TSB and Agar. Plated Petri dishes are then incubated at 37 °C for 24 h before counting. Four~~
525 ~~Petri dishes, with two different dilution levels, are prepared, and then the number of the counted~~
526 ~~colonies are averaged, to retrieve the bacterial concentration in the solution and its statistical~~
527 ~~uncertainty. The dilution levels for plating were 10^{-4.5} and 10⁻⁵: these serial dilutions were selected~~
528 ~~to obtain a number of CFUs in the range 20-150.~~

529 For the experiments performed at ChAMBRé, the typical bacterial concentration in the inoculum
530 is 10⁷ CFU ml⁻¹: to reach this concentration, a further dilution step is needed (i.e., typically 1:10
531 or 1:5) before the injection (see Massabò et al, 2018 for details).

532 The concentration of the solution to be injected inside ChAMBRe is also controlled in terms of
533 total cells ml⁻¹ by Quantom Tx Microbial Cell Counter. The sample is prepared from the bacterial
534 suspension in physiological solution. In each single analysis, Quantom Tx acquires 10 visual fields
535 of the slide's counting chamber, which correspond to an approx. volume of 0.09 µl, to retrieve the
536 bacterial count. To evaluate if the exposure of Quantom Tx lamp degrades the fluorescent probe
537 (photobleaching) of total cells, we repeated the total cell counts inserting and ejecting 10 times the
538 same sample: the total count probe didn't show a particular sensitivity to the exposure to the
539 Quantom Tx lamp, and the ~~coefficient of variation~~ ~~relative standard deviation~~ turned out to be less
540 than 5%. Further details on the use of Quantom Tx counter are given in Supplement S4.

541 The bacteria suspension, properly diluted, is injected into the chamber volume mainly by using the
542 Sparging Liquid Aerosol Generator, SLAG, which ensured the better reproducibility in earlier tests
543 (Danelli et al., 2021). The injection phase typically lasts 5 minutes. Injection air flow and duration
544 are automatically controlled by a Mass Flow Controller (Bronkhorst, model F201C-FA) managed
545 via SCADA. In this way, 2 ml of bacterial suspension are nebulized inside ChAMBRe.

546 Experiments with *E. coli* ~~have were been~~ performed by active sampling via the Andersen impactor:
547 sampling time was progressively increased after the injection to collect a suitable number of CFUs.
548 ~~At time t = 0 (three minutes after the conclusion of the injection to allow proper~~
549 ~~mixing/homogenization inside the ChAMBRe volume), three petri were consecutively sampled.~~
550 ~~The variability on the CFUs collected on the three petri, calculated as the ratio between standard~~
551 ~~deviation and mean value, resulted equal to 12%.~~ Sampling time during *E. coli* experiments are
552 summarized in Table S2 in Supplement S5.

553 After the experiments in the simulation chamber, the plates sampled are incubated at 37 °C for 24
554 h. The CFUs are then counted and, in the experiments conducted by active sampling, the CFU cm⁻³
555 are calculated.

556 The possible correlation between bacteria viability and air quality can be investigated in terms of
557 change in bacteria viability due to the exposure to atmospheric pollutants. Effects on bacteria
558 viability are compared in relation to “baseline experiments”. In a baseline experiment, the viability
559 of airborne bacteria is measured at atmospheric pressure, with temperatures around 20°C and with
560 relative humidity around 60%: such values have been chosen to reproduce an environment suitable
561 for the survival of bacteria (Dunklin E.W. 1948; Cox C.S. 1966; Benbough J.E. 1967). During
562 baseline experiments, the bacteria's viability depended on their characteristics and experimental

563 procedures only. The baseline was assessed both in “dark” ([solar simulator off](#)) and “light” ([solar](#)
564 [simulator on](#)) conditions. With “light” condition, the Solar Simulator was used with the AM1.5
565 filter mounted (see 2.1) to reduce the UV radiation; several experiments were replicated with the
566 Solar Simulator lamp intensity set at 105% and 80% of the nominal value (i.e., the maximum and
567 minimum intensity level which guarantees stability without using neutral filters). Baseline
568 experiments, see Section 3, were particularly important also to assess the reproducibility and hence
569 the sensitivity of the whole procedure.

570 The baseline assessment was followed by a set of exploratory experiments with *E. coli* exposed to
571 selected pollutants. We measured the possible bacterial viability changes due to the exposure to
572 atmospheric conditions typically met in polluted urban areas. So far, *E. coli* was exposed to
573 different concentrations of NO and NO₂, two of the most common pollutants emitted by vehicular
574 and ship traffics (Seinfeld and Pandis, 1998; Monks et al., 2009; Pöschl and Shiraiwa, 2015;).

575

3. Results

The experiments performed to investigate the possible effects on bacteria viability due to the exposure to atmospheric pollutants, were conducted by following the same procedure adopted to assess the baseline and introducing inside ChAMBR_e the specific pollutant. During gas pollutant experiments, NO or NO₂ concentration was kept constant thanks to the feedback control system described in 2.1.3.

3.1 Baseline experiments with *E. coli* in dark conditions.

E. coli behaviour in a set of ~~baseline experiments~~ eight replicated experiments, led from separate cultures, was first determined in dark conditions. The average total concentration and standard deviation of *E. coli* inside the chamber at t = 0 ~~immediately after the injection~~ (three minutes after the conclusion of the injection to allow proper mixing/homogenization inside the ChAMBR_e volume) was (0.34 ± 0.083) cells cm⁻³, as measured by the WIBS; the average viable concentration and standard deviation, determined by the Andersen impactor sampling just after the injection at t = 0 (i.e., after 3 minutes of mixing time), was (0.04 ± 0.012) cells cm⁻³. The viable concentration at t = 0 was obtained by measuring the CFUs on three petri consecutively sampled; the coefficient of variation on the CFUs collected on the three petri, resulted equal to 12%.

The average ratio and standard deviation of viable:total (V:T in the following) bacteria concentration inside ChAMBR_e, at t = 0 ~~the beginning of the experiments therefore~~ turned out to be V:T = (0.13 ± 0.073) , ~~with the viable cells counted in terms of CFUs~~. The total and viable bacteria concentration values measured inside ChAMBR_e depended on the V:T ratio in the inoculum to be injected (biological effects between each bacteria culture) and on the aerosolization process affecting the bacteria viability. ~~However, it is worthy to note the stability of baseline results despite the variability of the V:T ratio measured in the bacteria inoculum before the injection (see figure 7 and 8).~~ The bacteria viable concentration in the inoculum was determined via standard dilution plating while the bacteria total concentration was calculated by the Quantum Tx. During baseline experiments, the V:T ratio of the inoculum ranged between 0.25 ± 0.03 and 0.50 ± 0.06 . Time-trends of the averaged total and viable concentration of the bacteria, nebulized inside ChAMBR_e, are shown in Figure 76. ~~Average values are the result of eight replicated experiments.~~ Bacteria lifetime in ChAMBR_e can be calculated by fitting the data of each ~~with experiment with~~ an exponential function as:

607

608

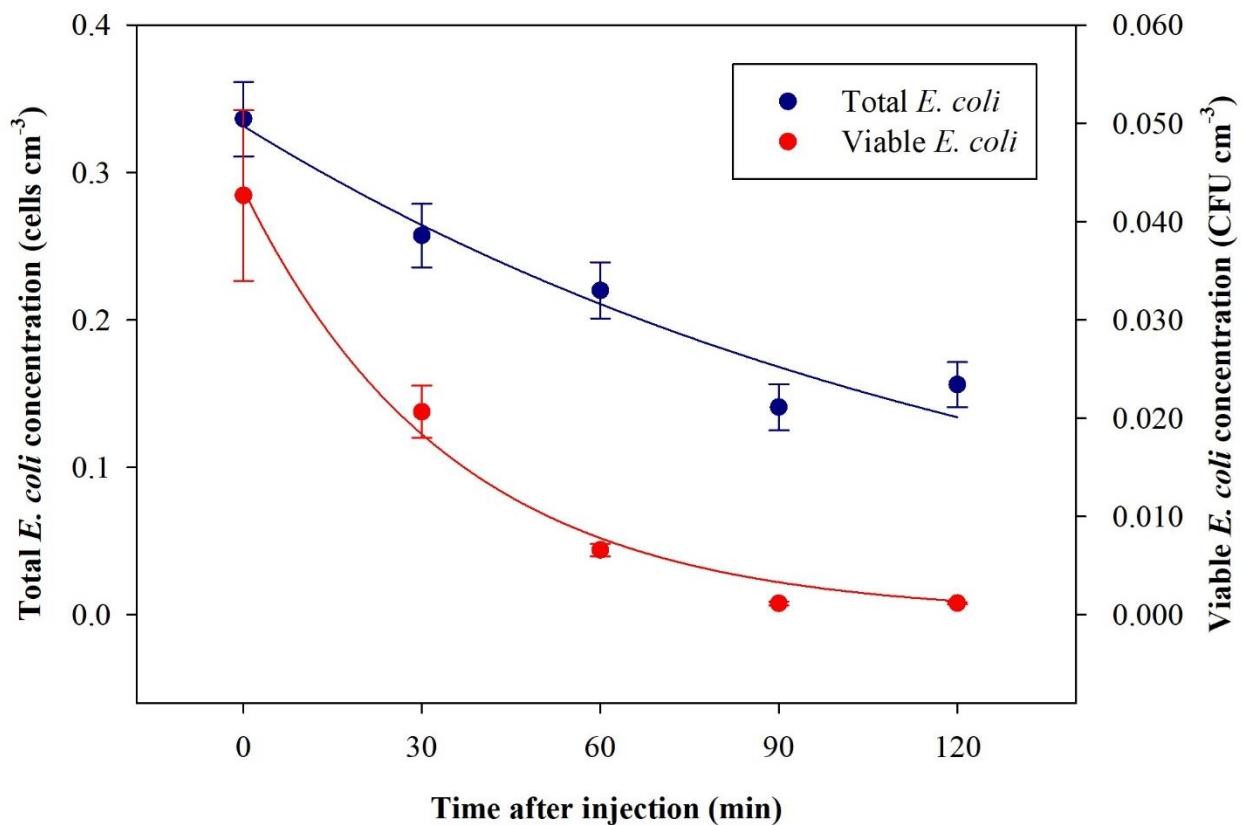
$$C(t) = C_0 e^{-\frac{t}{\tau}} \quad (2)$$

609

610 where C_0 is the ~~average of~~ total or viable concentration of *E. coli* just after the injection ($t = 0$) and

611 τ is the total or viable bacteria lifetime, respectively. In table 2, ~~the average and standard deviation~~

612 ~~of~~ C_0 and τ for the *E. coli* total and viable concentration of ~~eight experiments~~ *E. coli* are reported.



613

614 **Figure 7:** Time-trend of *E. coli* average bacteria total (~~red blue~~) and viable (~~redgreen~~) concentration inside

615 ChAMBR_e obtained by eight repetitions of baseline experiments.

616

617 **Table 2:** C_0 and τ (~~average \pm std deviation~~) of the exponential fit for total and viable concentration of *E. coli*.

Exponential function	Total <i>E. coli</i>	Viable <i>E. coli</i>
C_0	(0.33 \pm 0.082) cells cm ⁻³	(0.043 \pm 0.002) CFU cm ⁻³
τ (min)	15325 \pm 1622	324 \pm 45

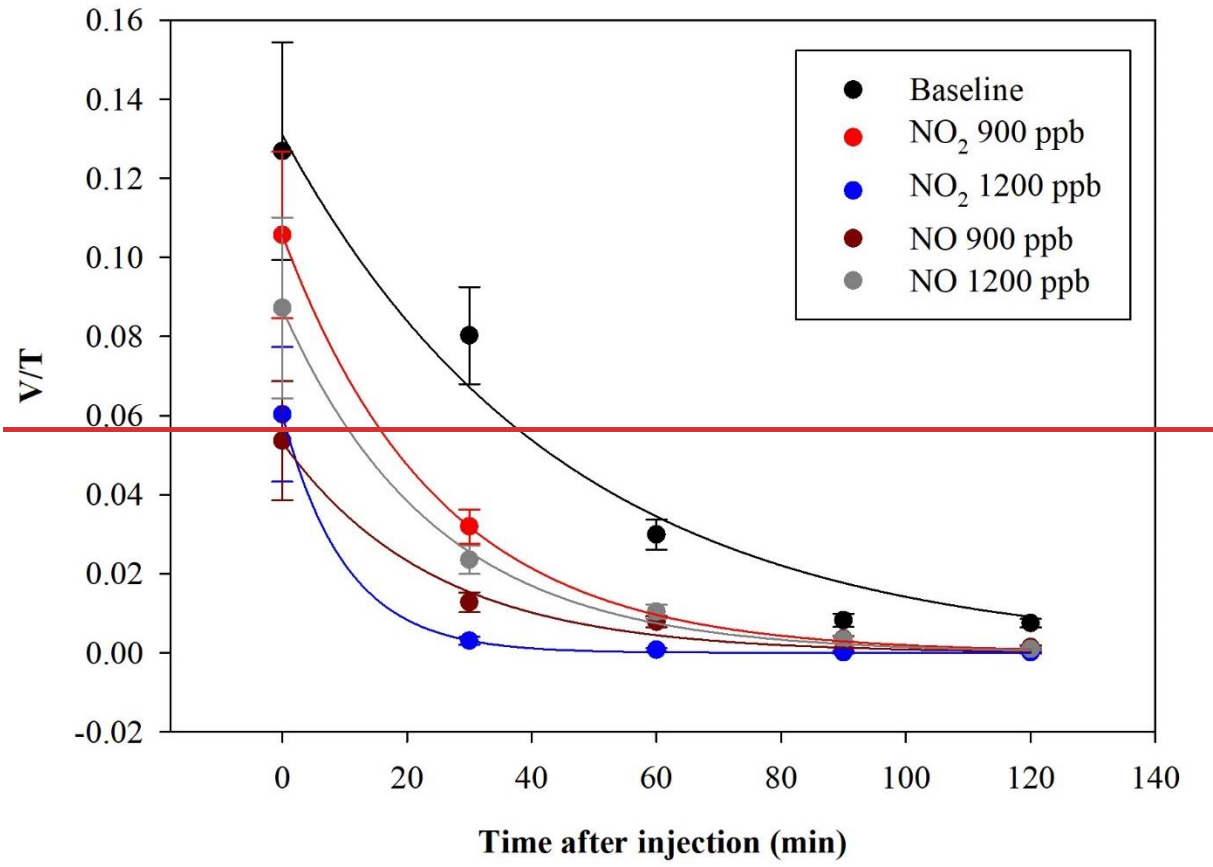
618

619 The total *E. coli* averaged lifetime is about ~~125~~150 minutes; this value agrees with data reported
620 in (Massabò et al., 2018) for generic aerosols: particles in the same size range of *E. coli* (1-2 μm)
621 and $\tau = 2-3$ hours ~~partieles, in the size range of 1—2 μm ($\tau = 2-3$ hours), the same of *E. coli*~~. The
622 viable *E. coli* averaged lifetime is about ~~32~~4 minutes, lower than the aerodynamic lifetime, this
623 indicating the difficulty of this microorganism to survive in the atmospheric medium.

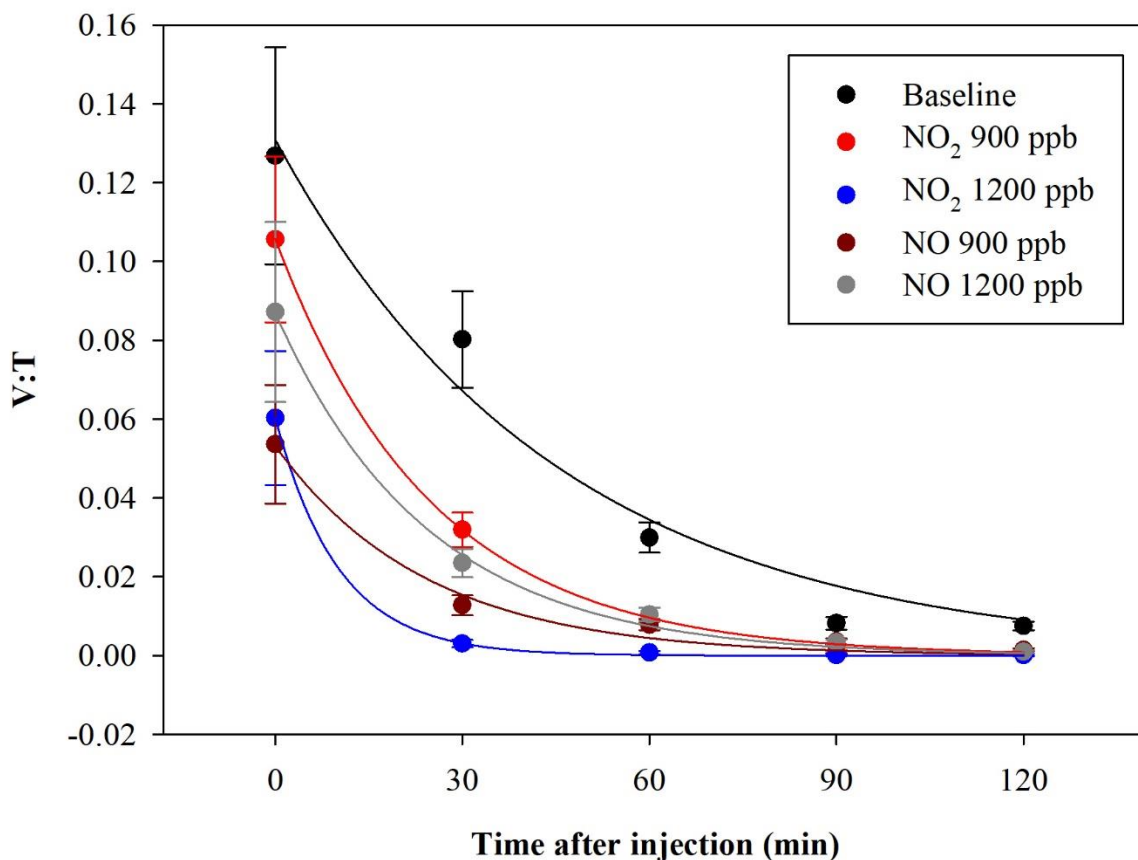
624 *3.2 Experiments with E. coli and NO_x in dark conditions.*

625 A preliminary check was performed exposing the *E. coli* to O₃, which is recognized to be a strong
626 antimicrobial agent (Kim et al., 1999; Giuliani et al., 2018; Thanomsub et al., 2022), hence the
627 expected result was a complete viability loss. The exposure of bacteria to O₃ (concentration > 1000
628 ppb) resulted in a roughly complete cell mortality, as expected. The initial condition immediately
629 after the injection was V:T = (0.03 \pm 0.01) and no CFUs were collected in any of the following
630 samplings (starting 30 minutes after the injection).

631 ~~Then~~In another experimentsexperiments, bacteria were exposed to NO₂ and NO concentrations,
632 900 and 1200 ppb for both the pollutants. The exposure of bacteria to such pollutants showed a
633 V:T reduction. The average results, obtained in a set of eight experiments, led from separate
634 cultures, are shown in Figure 8.



635



636

637 **Figure 8:** Time-trend of the V:T ratio for *E. coli* in baseline (black) and in the experiments with ChAMBR_e maintained
 638 at a constant concentration of: NO₂ (900 ppb red and 1200 ppb blue) and NO (900 ppb dark red and 1200 ppb gray).

639 The quantitative reduction in the *E. coli* lifetime, due to the exposure to pollutants, can be evaluated
 640 considering the V:T ratio and fitting the data with an exponential curve, as previously described;
 641 the results are shown in Table 3.

642 **Table 3:** Initial values and τ (average and std deviation) of the exponential fit for V:T ratio of *E. coli* at different
 643 pollutant concentrations.

Exponential function	(V:T t=0)	τ (min)
Baseline	0.13 ± 0.01	45 ± 6
NO ₂ 900 ppb	0.106 ± 0.001	25 ± 1
NO ₂ 1200 ppb	0.0603 ± 0.0003	10.1 ± 0.4
NO 900 ppb	0.053 ± 0.003	24 ± 3

NO 1200 ppb	0.087 ± 0.002	24 ± 2	
<u>Exponential function</u>	<u>(V:T t = 0)</u>	<u>τ (min)</u>	<u>N. of experiments #</u>
<u>Baseline</u>	<u>0.13 ± 0.07</u>	<u>40 ± 5</u>	<u>8</u>
<u>NO₂ 900 ppb</u>	<u>0.11 ± 0.02</u>	<u>25 ± 2</u>	<u>2</u>
<u>NO₂ 1200 ppb</u>	<u>0.06 ± 0.02</u>	<u>11 ± 2</u>	<u>2</u>
<u>NO 900 ppb</u>	<u>0.05 ± 0.01</u>	<u>26 ± 3</u>	<u>2</u>
<u>NO 1200 ppb</u>	<u>0.10 ± 0.02</u>	<u>25 ± 4</u>	<u>2</u>

644

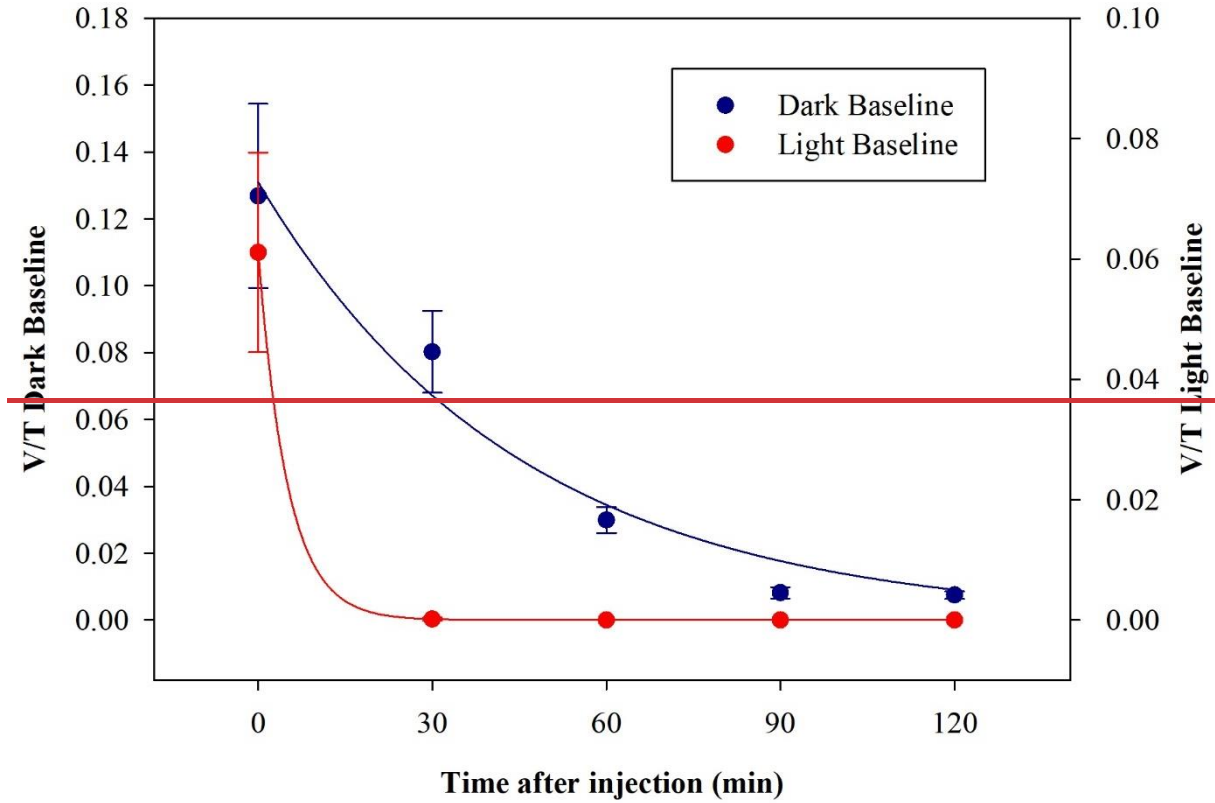
645 *E. coli* averaged lifetime in baseline experiments, calculated on the V:T ratio, turned out to be
646 about 405 min. The exposure of *E. coli* to NO₂ reduced the lifetime to about 25 and 110 min with
647 a concentration of 900 ppb and 1200 ppb respectively. The exposure to 900 ppb and 1200 ppb of
648 NO decreased bacteria lifetime to 26 and 25 min, respectively and the values are similar 24 min
649 for both concentrations and they are equal to the value obtained with the lowest NO₂
650 concentration. ‡ The increase of the NO concentration did not correspond to a decrease in the *E.*
651 *coli* viability, as observed with NO₂: these results suggests a greater toxic effect of NO₂ than of
652 NO on that NO₂ is more toxic for *E. coli* than NO. In addition, the increase of the NO concentration
653 did not correspond to a decrease in the *E. coli* viability, as observed with NO₂. The literature of a
654 comparison of the toxic effects of NO and NO₂ on *E coli* is poor.- Some research articles have
655 demonstrated negative effects of these two gases on bacterial strains: Kosaka et al 1986 found a
656 decrease in *E.coli* viability with increasing NO₂ concentration. Janvier et al, 2020 highlighted a
657 significant adverse effect of NO₂ on some commensal skin bacterial strains. Mancinelli and
658 McKay, 1983 found that a low concentration of NO is bacteriostatic for some organisms but not
659 for others. † It is worth noting that NO has a strong antimicrobial property, being an endogenously
660 produced molecule that is critical for critical infection defence (Fang, 1997), although some
661 bacteria are able to escape this NO action (Privett et al., 2012).

662

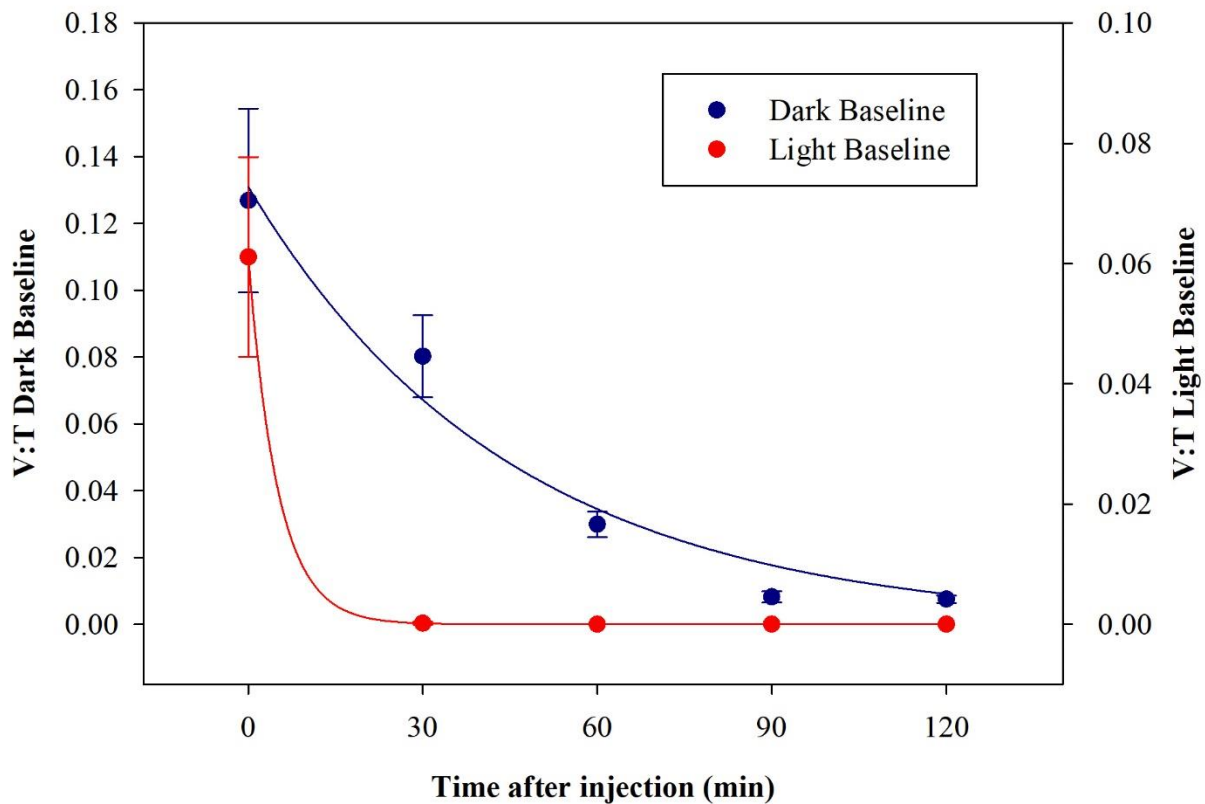
663 3.2 Experiments with *E. coli* and Solar Simulator.

664 *E. coli* behavior when exposed to light was determined in a set of dedicated baseline experiments.
665 No significant differences in results appeared changing the intensity of the Solar Simulator
666 operated with the AM1.5G filter and the data with a Solar Simulator intensity of 100% are here

667 ~~reported~~~~gathered~~. After the injection, the average total concentration of *E. coli* reached inside the
668 chamber was (0.30 ± 0.03) cells cm^{-3} , compatible with the dark baseline; while the average viable
669 concentration was (0.019 ± 0.005) cells cm^{-3} , lower than what obtained in dark experiments. The
670 consequent V:T ratio was (0.06 ± 0.02) . The viable concentration collapses quickly, reaching zero
671 after 30 minutes~~after 30 minutes~~, $V:T = (4.7 \pm 7.1) \cdot 10^{-5}$ cells cm^{-3} and reaches zero after an hour.
672 The comparison between V:T ratio obtained for dark and light baseline is shown in Figure 89.



673



674

675 **Figure 9:** Time-trend of the V:T ratio for *E. coli* in the dark baseline (dark blue) and light baseline (red) experiments.

676

677 These results indicate a significant decrease in bacteria viability due to their exposure to solar
 678 radiation. The behavior, here evaluated in atmospheric environment, agrees with observation in
 679 water environments reported in several works (Whitman et al., 2004; Jozić et al., 2014; Tiwari et
 680 al., 2022); the solar radiation is indicated as an abiotic factor with the negative effect of bringing
 681 some bacteria strains, among which *E. coli*, into a temporary inactivation/non-cultivable state.

682

683 **4. Discussion, conclusion and perspectives**

684 The main result presented in this work is the assessment of a multi-step and well controlled
 685 protocol to perform experiments on the impact of air quality on bacteria viability by an atmospheric
 686 simulation chamber, ChAMBRe in this case. Even if the chamber configuration is still in progress
 687 and several new equipment will be deployed at ChAMBRe in the ~~next~~near future, the present set-
 688 up opens the possibility of systematic studies. The average τ of the V:T ratio of eight baseline
 689 experiments was 40 min with a standard deviation of 5 min; \mp the coefficient of variation of 13%

690 ~~reproducibility of the baseline reference, based on the active bacteria sampling by a one stage~~
691 ~~Andersen impactor, turned out to be at the 20% level and this~~ corresponds to the experimental
692 sensitivity ~~to~~for changes in ~~the~~ *E. coli* viability due to exposure to pollutants and/or other relevant
693 parameters. The baseline reference must be experimentally determined for each bacteria strain and
694 efforts are planned for repeating the observation with *Bacillus subtilis*, *Bacillus spizizenii* and
695 *Pseudomonas fluorescens* in the ~~next~~near future. It is worthy to note that the experimental protocol
696 returns the lifetime of total and viable bacteria injected in the chamber. The figure for total bacteria
697 corresponds to the aerodynamic behavior of aerosol of diameter around 1 μm , already reported in
698 (Massabò et al., 2008) while the lifetime of viable bacteria is much shorter (about half an hour)
699 due to the difficulty of this microorganism to survive in the atmospheric medium. Such shorter
700 lifetime posed clear constraints on the first experiments with exposure of *E. coli* to NO_x inside
701 ChAMBRé. A time window of two hours after the bacteria injection was considered to observe
702 the behavior of *E. coli* viability and it was possible to quantify a lifetime reduction, in dark
703 conditions, clearly related to NO and NO_2 concentration inside ChAMBRé. These findings pave
704 the road to systematic studies including other bacteria strains and pollutant species. With the *E.*
705 *coli* exposed to the light produced by the Solar Simulator operated with the AM1.5 filter, the
706 viability resulted very short even in the baseline conditions and therefore no further experiment
707 with pollutants was performed. With other bacterial strains, the impact of light on viability will
708 have to be reinvestigated.

709 It is well known in the literature that the viable but non-culturable condition (VBNC) is a survival
710 strategy of many bacteria in the environment in response to adverse environmental conditions (e.g.,
711 solar radiation). There is a growing scientific interest in studying VBNC cells, including to
712 understand novel public health implications of VBNC cells. In our simulated experiments, we are
713 investigating alternative methods to detect bacterial viability and VBNC state, such as “live and
714 dead staining” by fluorescence microscopy. This assay can be used to monitor the viability of
715 bacterial populations as a function of cell membrane integrity using different fluorescent dyes.
716 Further experiments with “flow cytometry” could certainly be more beneficial not only to
717 enumerate live and dead bacteria, but also to evaluate the health and viability of bacterial cells by
718 determining the activity of bacterial oxidases and reductases.

719

5. Acknowledgments

We are indebted to the personnel of the mechanical workshop of the INFN division of Genoa for the continuous support in the development of the ChAMBRé structure. The development of the chamber and the deployment of the equipment was supported by several European and Italian projects/grants: EUROCHAMP2020 (H2020: Infrastructure Activity under grant agreement No 730997); PON per-ACTRIS-IT (MUR-IT: PON project PIR_00015 “Per ACTRIS IT”); BLUE-LAB NET (F.E.S.R. - FONDO EUROPEO DI SVILUPPO REGIONALE Azione POR, Regione Liguria, IT); ATMO-ACCESS (H2020: Infrastructure Activity under grant agreement No 101008004); NextGenerationEU PNRR-ITINERIS (Italian Integrated Environmental Research Infrastructures System). [The publication has been funded by EU - Next Generation EU Mission 4 “Education and Research” - Component 2: “From research to business” - Investment 3.1: “Fund for the realisation of an integrated system of research and innovation infrastructures” - Project IR0000032 – ITINERIS - Italian Integrated Environmental Research Infrastructures System - CUP B53C22002150006. The authors acknowledge the Research Infrastructures participating in the ITINERIS project with their Italian nodes: ACTRIS, ANAEE, ATLaS, CeTRA, DANUBIUS, DISSCO, e-LTER, ECORD, EMPHASIS, EMSO ,EUFAR ,Euro-Argo, EuroFleets, Geoscience, IBISBA, ICOS, JERICO, LIFEWATCH, LNS, N/R Laura Bassi, SIOS, SMINO.](#)

6. References

Akin, E., Pelen, N. N., Tiryaki, I. U., Yalcin, F.: Parameter identification for gompertz and logistic dynamic equations, PLoSONE15(4): e0230582, <https://doi.org/10.1371/journal.pone.0230582>, 2020.

~~Amato, P., Ménager, M., Sancelme, M., Laj, P., Mailhot, G., Delort, A. M.: Microbial population in cloud water at the Puy de Dôme: Implications for the chemistry of clouds, Atmos. Environ. 39, 4143–4153, <https://doi.org/10.1016/j.atmosenv.2005.04.002>, 2005.~~

~~Amato, P., Parazols, M., Sancelme, M., Laj, P., Mailhot, G., Delort, A. M.: Microorganisms isolated from the water phase of tropospheric clouds at the Puy de Dôme : major groups and growth abilities at low temperatures, FEMS Microbiol. Ecol. 59, 242–254, <https://doi.org/10.1111/j.1574-6941.2006.00199.x>, 2006.~~

752 Amato, P., Demeer, F., Melaouhi, A., Fontanella, S., Martin-Biesse, A.-S., Sancelme, M., Laj, P.,
753 Delort, A.-M.: A fate for organic acids, formaldehyde and methanol in cloud water: their
754 biotransformation by micro-organisms, *Atmospheric Chem. Phys.* 7, 4159–4169,
755 <https://doi.org/10.5194/acp-7-4159-2007>, 2007.

756 Amato, P., Joly, M., Schaupp, C., Attard, E., Möhler, O., Morris, C.E., Brunet, Y., Delort, A.-M.:
757 Survival and ice nucleation activity of bacteria as aerosols in a cloud simulation chamber,
758 *Atmospheric Chem. Phys.* 15, 6455–6465. <https://doi.org/10.5194/acp-15-6455-2015>, 2015.

759 [Amato, P., Mathonat, F., Nuñez Lopez, L., Péguilhan, R., Bourhane, Z., Rossi, F., Vyskocil, J.,](#)
760 [Joly, M., and Ervens, B.: The aeromicrobiome: the selective and dynamic outer-layer of the Earth's](#)
761 [microbiome, *Frontiers in Microbiology*, 14, <https://doi.org/10.3389/fmicb.2023.1186847>, 2023](#)

762 Annadurai, G., Rajesh Babu, S., Srinivasamoorthy, V. R.: Development of mathematical models
763 (Logistic, Gompertz and Richards models) describing the growth pattern of *Pseudomonas putida*
764 (NICM 2174), *Bioprocess Engineering*, 23(6), 607-612, <https://doi.org/10.1007/s004490000209>,
765 2000.

766 ~~Ariya, P.A., Nepotchatykh, O., Ignatova, O., Amyot, M. : Microbiological degradation of~~
767 ~~atmospheric organic compounds, *Geophysical Research Letters* 29, NO. 22, 2077,~~
768 ~~<https://doi.org/10.1029/2002GL015637>, 2002.~~

769 Ariya, P.A., Amyot, M.: New Directions: The role of bioaerosols in atmospheric chemistry and
770 physics, *Atmos. Environ.* 38, 1231–1232, <https://doi.org/10.1016/j.atmosenv.2003.12.006>, 2004.

771 Baty, F., Delignette-Muller, M. L. : Estimating the bacterial lag time : which model, which
772 precision?, *International journal of food microbiology*, 91(3), 261-277,
773 <https://doi.org/10.1016/j.ijfoodmicro.2003.07.002>, 2004.

774 ~~Bauer, H., Kasper Giebl, A., Zibuschka, F., Hitzenberger, R., Kraus, G. F., Puxbaum, H.:~~
775 ~~Determination of the Carbon Content of Airborne Fungal Spores, *Anal. Chem.*, 74, 1, 91–95,~~
776 ~~<https://doi.org/10.1021/ac010331+>, 2002.~~

777 [Bauer, H., Giebl, H., Hitzenberger, R., Kasper-Giebl, A., Reischl, G., Zibuschka, F., Puxbaum, H.:](#)
778 [Airborne bacteria as cloud condensation nuclei, *Journal of Geophysical Research*, vol. 108, no.](#)
779 [D21, 4658, doi:10.1029/2003JD003545, 2003.](#)

780 Benbough, J. E.: Death Mechanisms in Airborne *Escherichia coli*, *J. Gen. Microbiol.* 47, 325–
781 333, <https://doi.org/10.1099/00221287-47-3-325>, 1967.

782 Birch, C. P. D.: A new generalized logistic sigmoid growth equation compared with the Richards
783 growth equation, *Annals of botany*, 83(6), 713-723, <https://doi.org/10.1006/anbo.1999.0877>,
784 1999.

785 Brotto, P., Repetto, B., Formenti, P., Pangui, E., Livet, A., Bousserhine, N., Martini, I., Varnier,
786 O., Doussin, J.F., Prati, P.: Use of an atmospheric simulation chamber for bioaerosol investigation:
787 a feasibility study, *Aerobiologia* 31, 445–455, <https://doi.org/10.1007/s10453-015-9378-2>, 2015.

788 ~~Bowers, R. M., McLetchie, S., Knight, R., Fierer, N.: Spatial variability in airborne bacterial~~
789 ~~communities across land use types and their relationship to the bacterial communities of potential~~
790 ~~source environments. ISME J. 5, 601–612, <https://doi.org/10.1038/ismej.2010.167>, 2011.~~

791 Bundke, U., Reimann, B., Nillius, B., Jaenicke, R., Bingemer, H.: Development of a Bioaerosol
792 single particle detector (BIO IN) for the Fast Ice Nucleus CHamber FINCH, Atmos. Meas. Tech.,
793 3, 263–271, <https://doi.org/10.5194/amt-3-263-2010>, 2010.

794 Burrows, S. M., Butler, T., Jöckel, P., Tost, H., Kerkweg, A., Pöschl, U., Lawrence, M.G.: Bacteria
795 in the global atmosphere – Part 2: Modeling of emissions and transport between different
796 ecosystems, Atmospheric Chem. Phys. 9, 9281–9297. <https://doi.org/10.5194/acp-9-9281-2009>,
797 2009.

798 Chou, C., Stetzer, O., Weingartner, E., Jurányi, Z., Kanji, Z. A., Lohmann, U.: Ice nuclei properties
799 within a Saharan dust event at the Jungfraujoch in the Swiss Alps, Atmos. Chem. Phys., 11, 4725–
800 4738, <https://doi.org/10.5194/acp-11-4725-2011>, 2011.

801 CID, Commission Implementing Decision (EU) 2023/900, “Setting up the Aerosol, Clouds and
802 Trace Gases Research Infrastructure (ACTRIS ERIC)” Official Journal of the European Union
803 L115/15, 03/05/2023.

804 Cox, C.S.: The Survival of *Escherichia coli* sprayed into Air and into Nitrogen from Distilled
805 Water and from Solutions of Protecting Agents, as a Function of Relative Humidity, J. Gen.
806 Microbiol. 43, 383–399, <https://doi.org/10.1099/00221287-43-3-383>, 1966.

807 Danelli, S., Brunoldi, M., Massabò, D., Parodi, F., Vernocchi, V., Prati, P.: Comparative
808 characterization of the performance of bio-aerosol nebulizers in connection with atmospheric
809 simulation chambers. Atmos. Meas. Tech., 14, 4461–4470, [https://doi.org/10.5194/amt-14-4461-](https://doi.org/10.5194/amt-14-4461-2021)
810 2021, 2021.

811 Deguillaume, L., Leriche, M., Amato, P., Ariya, P.A., Delort, A.-M., Pöschl, U., Chaumerliac, N.,
812 Bauer, H., Flossmann, A.I., Morris, C.E.: Microbiology and atmospheric processes: chemical
813 interactions of primary biological aerosols, Biogeosciences 5, 1073–1084,
814 <https://doi.org/10.5194/bg-5-1073-2008>, 2008.

815 ~~[Delort, A. M., Vaitilingom, M., Amato, P., Sancelme, M., Parazols, M., Mailhot, G., Laj, P.,](https://doi.org/10.1016/j.atmosres.2010.07.004)~~
816 ~~[Deguillaume, L.: A short overview of the microbial population in clouds: Potential roles in](https://doi.org/10.1016/j.atmosres.2010.07.004)~~
817 ~~[atmospheric chemistry and nucleation processes, Atmospheric Research, Volume 98, Issues 2–4,](https://doi.org/10.1016/j.atmosres.2010.07.004)~~
818 ~~[Pages 249-260, <https://doi.org/10.1016/j.atmosres.2010.07.004>, 2010](https://doi.org/10.1016/j.atmosres.2010.07.004)~~

819 Després, V. R., Huffman, J. A., Burrows, S. M., Hoose, C., Safatov, A. S., Buryak, G., Fröhlich-
820 Nowoisky, J., Elbert, W., Andreae, M.O., Pöschl, U., Jaenicke, R.: Primary biological aerosol
821 particles in the atmosphere: a review. Tellus B Chem. Phys. Meteorol. 64, 15598,
822 <https://doi.org/10.3402/tellusb.v64i0.15598>, 2012.

823 Dunklin, E. W., Puck, T. T.: The lethal effect of relative humidity on airborne bacteria. J. Exp.
824 Med. 87, 87–101, <https://doi.org/10.1084/jem.87.2.87>, 1948.

825 [Ehrlich, R., Miller, S., and Walker, R. L.: Relationship Between Atmospheric Temperature and](#)
826 [Survival of Airborne Bacteria, *Appl Microbiol*, 19, 245–249, 1970.](#)

827 [Ervens, B. and Amato, P.: The global impact of bacterial processes on carbon mass. *Atmos. Chem.*
828 \[Phys.\]\(#\), 20, 1777–1794, <https://doi.org/10.5194/acp-20-1777-2020>, 2020.](#)

829 [Fang, F. C.: Perspectives series: host/pathogen interactions. Mechanisms of nitric oxide-related](#)
830 [antimicrobial activity, *J Clin Invest*. 99\(12\): 2818–2825, <https://doi.org/10.1172%2FJCI119473>,](#)
831 [1997.](#)

832 [Fankhauser, A. M., Antonio, D. D., Krell, A. M., Alston, S. J., Banta, S., and McNeill, V. F.:](#)
833 [Constraining the impact of bacteria on the aqueous atmospheric chemistry of small organic](#)
834 [compounds, *ACS Earth Space Chem.*, <https://doi.org/10.1021/acsearthspacechem.9b00054>, 2019.](#)

835 Fröhlich-Nowoisky, J., Kampf, C. J., Weber, B., Huffman, J. A., Pöhlker, C., Andreae, M. O.,
836 Lang-Yona, N., Burrows, S. M., Gunthe, S. S., Elbert, W., Su, H., Hoor, P., Thines, E., Hoffmann,
837 T., Després, V. R., Pöschl, U.: Bioaerosols in the Earth system: Climate, health, and ecosystem
838 interactions. *Atmospheric Res.* 182, 346–376, <https://doi.org/10.1016/j.atmosres.2016.07.018>,
839 2016.

840 Giuliani, G., Ricevuti, G., Galoforo, A., Franzini, M.: Microbiological aspects of ozone:
841 bactericidal activity and antibiotic/antimicrobial resistance in bacterial strains treated with ozone.
842 *Ozone Therapy*, 3(3), <https://doi.org/10.4081/ozone.2018.7971>, 2018.

843 [Gong, J., Qi, J., E, B., Yin, Y., Gao, D.: Concentration, viability and size distribution of bacteria](#)
844 [in atmospheric bioaerosols under different types of pollution. *Environmental Pollution* 257,](#)
845 [113485, <https://doi.org/10.1016/j.envpol.2019.113485>, 2020.](#)

846 [Griffin, D., Westphal, D., Gray, M.: Airborne microorganisms in the African desert dust corridor](#)
847 [over the mid Atlantic ridge, *Ocean Drilling Program, Leg 209, Aerobiologia* 22, 211–226,](#)
848 [https://doi.org/10.1007/s10453-006-9033-z, 2006.](#)

849 Hall, B. G., Acar, H., Nandipati, A., Barlow, M.: Growth Rates Made Easy, *Mol. Biol. Evol.* 31,
850 232–238, <https://doi.org/10.1093/molbev/mst187>, 2014.

851 [Jaber, S., Lallement, A., Sancelme, M., Lereboure, M., Mailhot, G., Ervens, B., and Delort, A.-](#)
852 [M.: Biodegradation of phenol and catechol in cloud water: comparison to chemical oxidation in](#)
853 [the atmospheric multiphase system, *Atmospheric Chemistry and Physics*, 20, 4987–4997,](#)
854 [https://doi.org/10.5194/acp-20-4987-2020, 2020.](#)

855 [Jaber, S., Joly, M., Brissy, M., Lereboure, M., Khaled, A., Ervens, B., and Delort, A.-M.: Biotic](#)
856 [and abiotic transformation of amino acids in cloud water: experimental studies and atmospheric](#)
857 [implications, *Biogeosciences*, 18, 1067–1080, <https://doi.org/10.5194/bg-18-1067-2021>, 2021.](#)

858 Jang, J., Hur, H.-G., Sadowsky, M. J., Byappanahalli, M. N., Yan, T., Ishii, S.: Environmental
859 *Escherichia coli*: ecology and public health implications-a review, *J. Appl. Microbiol.* 123, 570–
860 581, <https://doi.org/10.1111/jam.13468>, 2017.

861 [Janvier, X., Alexandre, S., Boukerb, A. M., Souak, D., Maillot, O., Barreau, M., Gouriou, F.,](#)
862 [Grillon, C., Feuilloley, M. G. J., Groboillot, A.: Deleterious Effects of an Air Pollutant \(NO₂\) on](#)
863 [a Selection of Commensal Skin Bacterial Strains, Potential Contributor to Dysbiosis?, *Frontiers of*](#)
864 [in Microbiology, Volume 11, Article 591839, <https://doi.org/10.3389/fmicb.2020.591839>, 2020.](#)
865

866 Jozić, S., Morović, M., Šolić, M., Krstulović, N., Ordulj, M.: Effect of solar radiation, temperature
867 and salinity on the survival of two different strains of *Escherichia coli*, *Fresenius Environ. Bull.*
868 23, 1852–1859, 2014.

869 [Khaled, A., Zhang, M., Amato, P., Delort, A.-M., and Ervens, B.: Biodegradation by bacteria in](#)
870 [clouds: an underestimated sink for some organics in the atmospheric multiphase system,](#)
871 [Atmospheric Chemistry and Physics, 21, 3123–3141, <https://doi.org/10.5194/acp-21-3123-2021>,](#)
872 [2021.](#)

873 [Krumins, V., Mainelis, G., Kerkhof, L. J., and Fennell, D. E.: Substrate-Dependent rRNA](#)
874 [Production in an Airborne Bacterium, *Environ. Sci. Technol. Lett.*, 1, 376–381,](#)
875 [https://doi.org/10.1021/ez500245y, 2014.](#)

876 ~~Tjørve, K. M. C., Tjørve, E.: The use of Gompertz models in growth analyses, and new Gompertz-~~
877 ~~model approach: An addition to the Unified Richards family, *PLOS ONE* June 5, 2017,~~
878 ~~<https://doi.org/10.1371/journal.pone.0178691>, 2017.~~

879 Kim, J. G., Yousef, A. E., Dave, S.: Application of Ozone for Enhancing the Microbiological
880 Safety and Quality of Foods: A Review, *Journal of Food Protection*, 62, 9, 1071-1087,
881 <https://doi.org/10.4315/0362-028X-62.9.1071>, 1999.

882 Kolbe, U., Yi, B., Poth, T., Saunders, A., Boutin, S., Dalpke, A. H.: Early Cytokine Induction
883 Upon *Pseudomonas aeruginosa* Infection in Murine Precision Cut Lung Slices Depends on Sensing
884 of Bacterial Viability, *Frontiers in Immunology* 2020, 11:598636,
885 <https://doi.org/10.3389/fimmu.2020.598636>, 2020.

886 [Kosaka, H., Yamamoto, H., Oda, Y., Uozumi, M: Induction of SOS functions by nitrogen dioxide](#)
887 [in *Escherichia coli* with different DNA-repair capacities, *Mutat Res. Aug; 162\(1\):1-5, doi:*](#)
888 [10.1016/0027-5107\(86\)90065-5, 1986.](#)

889 Lee, B. U., Kim, S. H., Kim, S. S.: Hygroscopic growth of *E. coli* and *B. subtilis* bioaerosols,
890 *Journal of Aerosol Science* 33, 1721–1723, [https://doi.org/10.1016/S0021-8502\(02\)00114-3](https://doi.org/10.1016/S0021-8502(02)00114-3),
891 2002.

892 Lee, B. U., Kim, S. S.: Sampling *E. coli* and *B. subtilis* bacteria bioaerosols by a new type of
893 impactor with a cooled impaction plate, *J. Aerosol Sci.*, 34, 1097–1100, 2003.

894 Lieberherr, G., Auderset, K., Calpini, B., Clot, B., Crouzy, B., Gysel-Ber, M., Konzelmann, T.,
895 Manzano, J., Mihajlovic, A., Moallemi, A., O'Connor, D., Sikoparija, B., Sauvageat, E., Tummon,
896 F., Vasilatou, K: Assessment of real-time bioaerosol particle counters using reference chamber
897 experiments, *Atmos. Meas. Tech.*, 14, 7693–7706, <https://doi.org/10.5194/amt-14-7693-2021>,
898 2021.

899 [Lighthart, B., Shaffer, B.T., Marthi, Ganio, L. M.: Artificial wind-gust liberation of microbial](#)
900 [bioaerosols previously deposited on plants. *Aerobiologia* 9, 189–196,](#)
901 <https://doi.org/10.1007/BF02066261>, 1993

902 ~~[Lighthart, B.: The ecology of bacteria in the al fresco atmosphere, *FEMS Microbiol. Ecol.* 23, 263–](#)~~
903 ~~<https://doi.org/10.1111/j.1574-6941.1997.tb00408.x>, 2006.~~

904 [Mancinelli, R. L. and McKay, C.P.: Effects of Nitric Oxide and Nitrogen Dioxide on Bacterial](#)
905 [Growth, Applied and Environmental Microbiology, 198–202,](#)
906 <https://doi.org/10.1128/aem.46.1.198-202.1983>, 1983.

907

908 Mainelis, G., Berry, D., Reoun An, H., Yao, M., DeVoe, K., Fennell, D.E., Jaeger, R.: Design and
909 performance of a single-pass bubbling bioaerosol generator, *Atmos. Environ.* 39, 3521– 3533,
910 <https://doi.org/10.1016/j.atmosenv.2005.02.043>, 2005.

911 Martiny, J. B. H., Bohannon, B. J. M., Brown, J. H., Colwell, R. K., Fuhrman, J. A., Green, J. L.,
912 Horner-Devine, M. C., Kane, M., Krumins, J. A., Kuske, C. R., Morin, P. J., Naeem, S., Ovreås,
913 L., Reysenbach, A.-L., Smith, V. H., Staley, J. T.: Microbial biogeography: putting
914 microorganisms on the map. *Nat. Rev. Microbiol.* 4, 102–112,
915 <https://doi.org/10.1038/nrmicro1341>, 2006.

916 Massabò, D., Danelli, S. G., Brotto, P., Comite, A., Costa, C., Di Cesare, A., Doussin, J. F.,
917 Ferraro, F., Formenti, P., Gatta, E., Negretti, L., Oliva, M., Parodi, F., Vezzulli, L., Prati, P.:
918 ChAMBRé: a new atmospheric simulation chamber for aerosol modelling and bio-aerosol
919 research, *Atmos. Meas. Tech.*, 11, 5885–5900, <https://doi.org/10.5194/amt-11-5885-2018>, 2018.

920 [Mayol, E., Jiménez, M. A., Herndl, G. J., Duarte, C. M., and Arrieta, J. M.: Resolving the](#)
921 [abundance and air-sea fluxes of airborne microorganisms in the North Atlantic Ocean. *Frontiers*](#)
922 [in *Microbiology*, 5, https://doi.org/10.3389/fmicb.2014.00557, 2014.](#)

923 Möhler, O., DeMott, P. J., Vali, G., Levin, Z.: Microbiology and atmospheric processes: the role
924 of biological particles in cloud physics, *Biogeosciences* 4, 1059–1071, [https://doi.org/10.5194/bg-](https://doi.org/10.5194/bg-4-1059-2007)
925 [4-1059-2007](https://doi.org/10.5194/bg-4-1059-2007), 2007.

926 Monks, P. S., Granier, C., Fuzzi, S., Stohl, A., Williams, M. L., Akimoto, H., Amann, M.,
927 Baklanov, A., Baltensperger, U., Bey, I., Blake, N., Blake, R. S., Carslaw, K., Cooper, O. R.,
928 Dentener, F., Fowler, D., Fragkou, E., Frost, G. J., Generoso, S., Ginoux, P., Grewe, V., Guenther,
929 A., Hansson, H. C., Henne, S., Hjorth, J., Hofzumahaus, A., Huntrieser, H., Isaksen, I. S. A.,
930 Jenkin, M. E., Kaiser, J., Kanakidou, M., Klimont, Z., Kulmala, M., Laj, P., Lawrence, M. G., Lee,
931 J. D., Liousse, C., Maione, M., McFiggans, G., Metzger, A., Mieville, A., Moussiopoulos, N.,
932 Orlando, J. J., O’Dowd, C. D., Palmer, P. I., Parrish, D. D., Petzold, A., Platt, U., Pöschl, U.,
933 Prévôt, A. S. H., Reeves, C. E., Reimann, S., Rudich, Y., Sellegri, K., Steinbrecher, R., Simpson,
934 D., ten Brink, H., Theloke, J., van der Werf, G. R., Vautard, R., Vestreng, V., Vlachokostas, Ch.,
935 von Glasow, R.: Atmospheric composition change – global and regional air quality, *Atmos.*
936 *Environ.* 43, 5268–5350, <https://doi.org/10.1016/j.atmosenv.2009.08.021>, 2009.

937 Morris, C. E., Georgakopoulos, D. G., Sands, D. C.: Ice nucleation active bacteria and their
938 potential role in precipitation. *J. Phys. IV Proc.* 121, 87–103,
939 <https://doi.org/10.1051/jp4:2004121004>, 2004.

940 Morris, C. E., Leyronas, C., Nicot, P. C.: Movement of Bioaerosols in the Atmosphere and the
941 Consequences for Climate and Microbial Evolution, in: Colbeck, I., Lazaridis, M. (Eds.), *Aerosol*
942 *Science: Technology and Applications*. John Wiley & Sons, Ltd, Chichester, UK, pp. 393–415,
943 <https://doi.org/10.1002/9781118682555.ch16>, 2014.

944 Mytilinaios, I., Salih, M., Schofield, H. K., Lambert, R. J. W.: Growth curve prediction from
945 optical density data, *Int. J. Food Microbiol.* 154, 169–176,
946 <https://doi.org/10.1016/j.ijfoodmicro.2011.12.035>, 2012.

947 Pöschl, U.: Atmospheric Aerosols: Composition, Transformation, Climate and Health Effects,
948 *Angew. Chem. Int. Ed.* 44, 7520–7540, <https://doi.org/10.1002/anie.200501122>, 2005.

949 Pöschl, U., Shiraiwa, M.: Multiphase Chemistry at the Atmosphere–Biosphere Interface
950 Influencing Climate and Public Health in the Anthropocene, *Chem. Rev.* 115, 4440–4475,
951 <https://doi.org/10.1021/cr500487s>, 2015.

952 [Privett, B. J., Broadnax, A. D., Bauman, S. J., Riccio, D. A., Schoenfisch, M. H.: Examination of](https://doi.org/10.1016/j.niox.2012.02.002)
953 [bacterial resistance to exogenous nitric oxide, *Nitric Oxide*, Volume 26, Issue 3, Pages 169-173,](https://doi.org/10.1016/j.niox.2012.02.002)
954 <https://doi.org/10.1016/j.niox.2012.02.002>, 2012.

955

956 ~~Prospero, J., Blades, E., Mathison, G., Naidu, R. : Interhemispheric transport of viable fungi and~~
957 ~~bacteria from Africa to the Caribbean with soil dust, *Aerobiologia* 21, 1–19,~~
958 ~~<https://doi.org/10.1007/s10453-004-5872-7>, 2005.~~

959 Romano, S., Di Salvo, M., Rispoli, G., Alifano, P., Perrone, M. R., Talà, A.: Airborne bacteria in
960 the Central Mediterranean: Structure and role of meteorology and air mass transport, *Science of*
961 *the Total Environment* 697 (2019) 134020, <https://doi.org/10.1016/j.scitotenv.2020.138899>, 2019.

962 Seinfeld, J. H., Pandis, S. N.: 1998. *Atmospheric Chemistry and Physics: From Air Pollution to*
963 *Climate Change*, Wiley-Interscience, ISBN 10: 04711178152 ISBN 13: 97804711178156, 1997.

964 Shaffer, B.T., Lighthart, B.: Survey of Culturable Airborne Bacteria at Four Diverse Locations in
965 Oregon: Urban, Rural, Forest, and Coastal, *Microb. Ecol.* 34, 167–177,
966 <https://doi.org/10.1007/s002489900046>, 1997.

967 Son, M. S., Taylor R. K.: Growth and Maintenance of *Escherichia coli* Laboratory Strains, *Curr.*
968 *Protoc.* 2021 January; 1(1): e20, <https://doi.org/10.1002/cpz1.20>, 2021.

969 Sun, J., Ariya, P.: Atmospheric organic and bio-aerosols as cloud condensation nuclei (CCN): A
970 review, *Atmos. Environ.* 40, 795–820, <https://doi.org/10.1016/j.atmosenv.2005.05.052>, 2006.

971 Thanomsub, B., Anupunpisit, V., Chanphetch, S., Watcharachaipong, T., Poonkhum, R., and
972 Srisukonth, C.: Effects of ozone treatment on cell growth and ultrastructural changes in bacteria,
973 *J. Gen. Appl. Microbiol.*, 48, 193–199, <https://doi.org/10.2323/jgam.48.193>, 2002.

974 [Tjørve, K. M. C., Tjørve, E.: The use of Gompertz models in growth analyses, and new Gompertz-](https://doi.org/10.1371/journal.pone.0178691)
975 [model approach: An addition to the Unified-Richards family, PLOS ONE June 5, 2017,](https://doi.org/10.1371/journal.pone.0178691)
976 [https://doi.org/10.1371/journal.pone.0178691, 2017.](https://doi.org/10.1371/journal.pone.0178691)

977 Tiwari, A., Kauppinen, A., Räsänen, P., Salonen, J., Wessels, L., Juntunen, J., Miettinen, I. T.,
978 Pitkänen, T.: Effects of temperature and light exposure on the decay characteristics of fecal
979 indicators, norovirus, and Legionella in mesocosms simulating subarctic river water, *Sci. Tot. Env.*
980 859, <https://doi.org/10.1016/j.scitotenv.2022.160340>, 2022.

981 ~~Tong, Y., Lighthart, B.: Diurnal Distribution of Total and Culturable Atmospheric Bacteria at a~~
982 ~~Rural Site. *Aerosol Sci. Technol.* 30, 246–254, <https://doi.org/10.1080/027868299304822>, 1999.~~

983 Vernocchi, V., Brunoldi, M., Danelli, S. G., Parodi, F., Prati, P., Massabò, D.: Characterization of
984 soot produced by the mini-inverted soot generator with an atmospheric simulation chamber,
985 *Atmos. Meas. Tech.*, 15, 2159–2175, <https://doi.org/10.5194/amt-15-2159-2022>, 2022.

986 Wagstrom, K. M., Pandis, S. N., Yarwood, G., Wilson, G. M., Morris, R. E.: Development and
987 application of a computationally efficient particulate matter apportionment algorithm in a three-
988 dimensional chemical transport model. *Atmos. Environ.* 42 (2008) 5650–5659,
989 <https://doi.org/10.1016/j.atmosenv.2008.03.012>, 2008.

990 Wang, C.-C., Fang, G.-C., Lee, L.: Bioaerosols study in central Taiwan during summer season,
991 *Toxicol. Ind. Health* 23, 133–139, <https://doi.org/10.1177/0748233707078741>, 2007.

992 Whitman, R. L., Nevers, M. B., Korinek, G.C., Byappanahalli, M.N.: Solar and temporal effects
993 on *Escherichia coli* concentration at a Lake Michigan swimming beach, *Appl Environ Microbiol.*
994 Vol 70, No. 7, <https://doi.org/10.1128/AEM.70.7.4276-4285.2004>, 2004.

995 [Wright, D. N., Bailey, G. D., and Goldberg, L. J.: Effect of Temperature on Survival of Airborne](https://doi.org/10.1128/AEM.70.7.4276-4285.2004)
996 [Mycoplasma pneumoniae, *J Bacteriol.* 99, 491–495, 1969.](https://doi.org/10.1128/AEM.70.7.4276-4285.2004)

997 Zwietering, M. H., Jongenburger, I., Rombouts, F. M., van 't Riet, K.: Modeling of the bacterial
998 growth curve, *Appl Environ Microbiol.* 1990 Jun; 56(6): 1875–1881, DOI:
999 <https://doi.org/10.1128/aem.56.6.1875-1881.1990>, 1990.